

Review

# Charged Lepton-Flavour Violation

Giulia Frau <sup>\*,†</sup>  and Christoph Langenbruch <sup>\*,†</sup>

Physikalisches Institut, Heidelberg University, 69120 Heidelberg, Germany

\* Correspondence: giulia.frau@cern.ch (G.F.); christoph.langenbruch@cern.ch (C.L.)

† These authors contributed equally to this work.

**Abstract:** We review the experimental status of searches for lepton-flavour violation in the charged sector. We give an overview of searches for lepton-flavour violation in purely leptonic decays, hadron decays, and decays of heavy bosons. We focus on the most stringent constraints on lepton-flavour violating processes in these areas and give prospects for ongoing and future experiments.

**Keywords:** standard model; flavour physics; lepton-flavour violation

## 1. Introduction

In the Standard Model (SM) with massless left-handed neutrinos, lepton flavour is conserved. However, lepton flavour in the SM is not protected by a fundamental symmetry but instead arises accidentally due to the absence of right-handed neutrinos. With the observation of neutrino oscillations [1,2], Lepton-Flavour Violation (LFV) has been established in the neutral sector. Extending the SM minimally by including right-handed neutrinos ( $\nu$ SM) also gives rise to Charged Lepton-Flavour Violating (CLFV) processes through loop-level diagrams involving neutrinos. These processes are, however, strongly suppressed by  $\sim(\Delta m_{ij}/M_W)^4$  through the GIM mechanism, resulting in branching fractions, e.g., for the decay  $\mu \rightarrow e\gamma$  of  $<10^{-54}$  [3–7]. Branching fractions of this size are well below the sensitivity of current and planned future experiments; any observation of CLFV decays would therefore constitute a clear sign of New Physics (NP) beyond the (minimally extended) SM.

Numerous NP models predict new sources of LFV, potentially resulting in enhancements of LFV branching fractions to observable rates, among them supersymmetric models, new heavy gauge bosons, extended Higgs sectors, and seesaw models. For a more detailed overview of NP models predicting CLFV effects, we refer the reader to Refs. [8,9].

Several excellent reviews exist in the area of CLFV, among them Refs. [8–13]. In this review, we focus on experimental aspects and the most recent results on CLFV. The review is structured in the following way. In Section 2 we introduce the major experiments that are currently performing searches for CLFV. Section 3 gives an overview of searches in decays of leptons, Section 4 details searches in hadron decays, and Section 5 discusses searches for CLFV in decays of heavy bosons. We conclude in Section 6.

## 2. Experiments and Experimental Techniques

The most stringent limits on CLFV decays are set in the muonic sector, using the decays  $\mu^+ \rightarrow e^+\gamma$  and  $\mu^+ \rightarrow e^+e^-e^+$ , as well as  $\mu^-N \rightarrow e^-N$  conversion. Current best limits in this area are provided by the MEG and SINDRUM (II) experiments [14–16]. Several future experiments are either under construction or planned with the aim to further improve these limits, among them MEG II [17], Mu3e [18] and Mu2e [19], COMET [20], and DeeMe [21]. The strongest limits in the search for LFV in  $\tau$  decays are set by the B-factories BaBar [22] and Belle [23], and by the LHCb experiment [24]. Future improvements in this area are expected from the Belle II experiment [25] and from LHCb [26]. The B-factories and LHCb also play a leading role in providing constraints on LFV hadron decays, including LFV



**Citation:** Frau, G.; Langenbruch, C. Charged Lepton-Flavour Violation. *Symmetry* **2024**, *16*, 359. <https://doi.org/10.3390/sym16030359>

Academic Editor: Giuseppe Latino

Received: 6 February 2024

Revised: 21 February 2024

Accepted: 10 March 2024

Published: 16 March 2024



**Copyright:** © 2024 by the authors. Licensee MDPI, Basel, Switzerland. This article is an open access article distributed under the terms and conditions of the Creative Commons Attribution (CC BY) license (<https://creativecommons.org/licenses/by/4.0/>).

decays of  $B$ - and  $D$ -mesons. The most stringent limits on the LFV decays of kaons are performed by BNL and KTeV [27,28]. Finally, the best limits on searches for LFV decays of Higgs and  $Z$  bosons are provided by ATLAS and CMS at the LHC [29,30].

In the following subsections, we will briefly introduce the experiments providing the most stringent bounds and discuss the experimental techniques exploited to search for CLFV. The experimental results are discussed in Sections 3–5 and summarized in Section 6.

### 2.1. MEG and MEG II

The MEG experiment, located at the Paul Scherrer Institut (PSI) in Switzerland, is designed for the search for the  $\mu^+ \rightarrow e^+\gamma$  decay [14,31]. A continuous beam of positive muons is stopped in a thin plastic target at the centre of a spectrometer, where they decay at rest. The signal decay  $\mu^+ \rightarrow e^+\gamma$  would result in the signature of a positron and a photon emitted back-to-back with energies of  $m_\mu/2 \sim 52.8 \text{ MeV}/c^2$ . A schematic view of the detector is given in Figure 1. The magnetic field for the spectrometer is provided by a thin-walled, superconducting solenoid with an axially graded magnetic field ranging from 1.27 T in the centre to 0.49 T at the ends of the magnet cryostat. A drift chamber system is used to reconstruct the positron trajectory and measure its momentum. Impact time and position of the positron are further measured with a timing counter consisting of scintillating bars. Photons are reconstructed using a liquid xenon scintillation detector, which provides excellent position, time, and energy resolution.

The MEG experiment took data from 2009 to 2013 and collected  $7.5 \times 10^{14}$  positive-muon decays with a muon beam intensity of  $3 \times 10^7 \mu^+/\text{s}$ . The upgraded detector MEG II is designed for a muon beam intensity of  $7 \times 10^7 \mu^+/\text{s}$  and provides improved position, momentum, and energy resolutions [17]. Data taking for the first MEG II physics run started in 2021 and the collaboration aims to reach the design sensitivity with the data taken until 2026 [32].

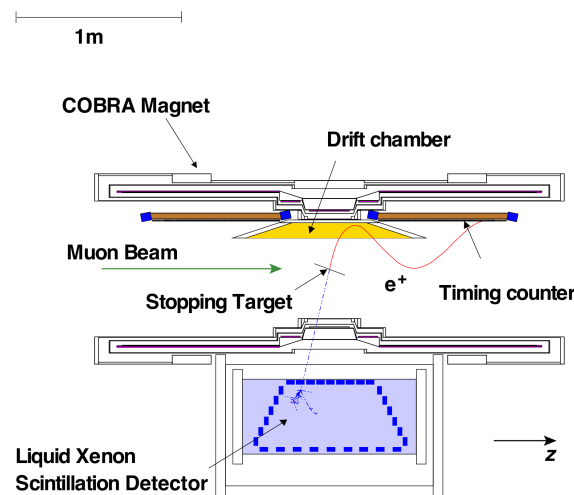


Figure 1. Schematic view of the MEG detector at PSI. Figure taken from Ref. [31].

### 2.2. SINDRUM and Mu3e

The main focus of the SINDRUM experiment, which operated at PSI from 1983 to 1986, was the search for the decay  $\mu^+ \rightarrow e^+e^-e^+$  [15]. A positive muon beam with momentum of 28 MeV/c and intensity of  $5 \times 10^6 \text{ s}^{-1}$  was stopped in a hollow double-cone-shaped target. The decay products were detected in a SINDRUM spectrometer, consisting of five concentric multi-wire proportional chambers located inside a magnet providing a field of  $B = 0.33 \text{ T}$ . The SINDRUM spectrometer covered a solid angle of  $\Omega/4\pi = 0.73$  and provided a momentum resolution of  $\Delta p/p = (12.0 \pm 0.4)\%$  (FWHM) for tracks of 50 MeV/c momentum.

The Mu3e experiment [18,33], currently under construction at PSI, aims to improve the sensitivity to the  $\mu^+ \rightarrow e^+e^-e^+$  decay by approximately four orders of magnitude with

respect to SINDRUM. A schematic view of the Mu3e experiment is shown in Figure 2. For the reduction of backgrounds from internal conversion ( $\mu^+ \rightarrow e^+e^-e^+\nu_e\bar{\nu}_\mu$ ), an excellent momentum resolution is paramount. To reduce accidental background that does not originate from a single decay vertex, good vertex and timing resolution is furthermore required. To minimize multiple scattering, thin silicon pixel detectors are used for tracking. These High-Voltage Monolithic Active Pixel Sensors (HV-MAPS) are based on HV-CMOS technology and can be thinned to  $50\ \mu\text{m}$  [34]. Precision timing is provided by timing detectors based on scintillating fibres and tiles. In the first phase of the experiment (Phase I), a muon rate of  $10^8\ \mu^+/s$  will be provided by the beamlines currently available at PSI. This will ensure an improvement on the current sensitivity of three orders of magnitude. In order to reach the ultimate sensitivity, a muon rate greater than  $10^9\ \mu^+/s$  is needed. For this purpose, the Mu3e experiment will exploit in the second phase the new High-Intensity Muon Beam (HiMB) facility, which is planned to be realised at PSI with the aim of delivering up to  $10^{10}\ \mu^+/s$  to experiments [35].

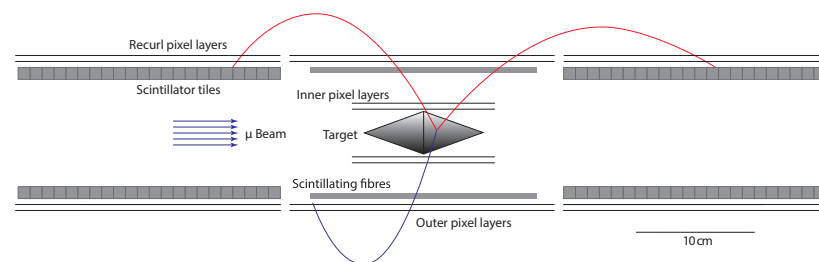


**Figure 2.** Schematic view of the Mu3e experiment in the Phase I configuration. Figure taken from Ref. [18].

### 2.3. SINDRUM II and Future $\mu^- N \rightarrow e^- N$ Experiments

The SINDRUM II experiment located at PSI was designed to search for conversions of a negative muon to an electron in the field of a nucleus [16]. If no neutrinos are emitted, this conversion represents a CLFV process, which results in a monoenergetic electron with  $E_{\mu e} = m_\mu c^2 - B_\mu - R$ , where  $B_\mu$  denotes the muon binding energy and  $R$  the atomic recoil. An overview of the SINDRUM II experiment is given in Figure 3. In order to separate background from muon decays in orbit ( $\mu^- N \rightarrow e^- \bar{\nu}_e \nu_\mu N$ ) from signal events, excellent momentum resolution is required for the electron. Two drift chambers (F and G in Figure 3) located inside a superconducting solenoid (H) are used to measure the helical trajectories of the electrons, resulting in a transverse momentum resolution of approximately 1% (FWHM). Two hodoscopes (D and E) are used for triggering and timing.

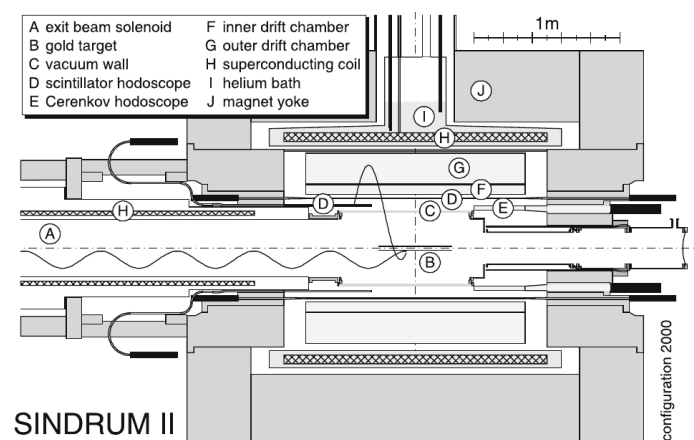


**Figure 3.** Overview of the SINDRUM II spectrometer. Figure taken from Ref. [36].

Three experiments are aimed at improving on the sensitivity of SINDRUM II: the Mu2e experiment [19], which is under construction at Fermilab, the COMET (COherent Muon-

to-Electron Transition) experiment [20] under construction at J-PARC, and the DeeMe (Direct emission of electron from Muon to electron conversion) experiment, also at J-PARC [21]. In contrast to SINDRUM II, which used the quasi-continuous (50 MHz) PSI proton accelerator beam, these experiments will use pulsed beams with longer pulse spacing. This will allow them to suppress prompt pion backgrounds (e.g., from radiative pion capture  $\pi^- N \rightarrow \gamma(\rightarrow e^+e^-)N^*$ ) by exploiting the shorter pion lifetime (26 ns at rest) compared to muons. The Mu2e experiment aims to reach a sensitivity of  $\mathcal{O}(10^{-17})$  in approximately three years of data taking using a thin aluminium target [19]. The COMET experiment is expected to reach a sensitivity of  $\mathcal{O}(10^{-15})$  in Phase I and a sensitivity of  $\mathcal{O}(10^{-17})$  in Phase II, also using an aluminium target [20]. The DeeMe experiment is expected to reach a sensitivity of  $\mathcal{O}(10^{-13})$  or  $\mathcal{O}(10^{-14})$  with a graphite or a silicon carbide target [21].

#### 2.4. The B-Factories and Belle II

The B-factories BaBar and Belle were located at the PEP-2 collider at SLAC and at the KEK-B collider at the KEK laboratory, respectively [22,23]. Both colliders were asymmetric  $e^+e^-$  colliders operating mainly on the  $\Upsilon(4S)$  resonance to produce  $B\bar{B}$  meson pairs with a production cross-section of approximately 1 nb. BaBar and Belle collected data corresponding to integrated luminosities of  $426 \text{ fb}^{-1}$  and  $711 \text{ fb}^{-1}$  at this centre-of-mass energy, which results in data sets of 471 M and 772 M  $B\bar{B}$  pairs, respectively. In addition to the large B-meson samples,  $\tau^+\tau^-$  pairs are also produced, with a production cross section of approximately  $0.9 \text{ nb}^{-1}$ , respectively. The B-factories are therefore well suited to search for the CLFV decays of B-mesons and  $\tau$ -leptons.

Belle II represents the major upgrade and successor of the Belle experiment, operating at SuperKEKB at KEK. The target instantaneous luminosity of SuperKEKB of  $8 \times 10^{35} \text{ cm}^{-2}\text{s}^{-1}$  is approximately a factor of 40 larger than at KEK-B [37]. The first physics data-taking period of Belle II with a fully instrumented detector started in 2019. Belle II plans to take a total data sample corresponding to an integrated luminosity of  $50 \text{ ab}^{-1}$ , approximately 50 times larger than the samples available from the B-factories [25].

A schematic view of the Belle II detector is shown in Figure 4. The Belle II detector covers the interaction region near hermetically. The innermost detector systems are the silicon pixel (PXD) and silicon strip (SVD) vertex detectors. Momentum and  $dE/dx$  measurements of charged particles are provided by the central drift chamber (CDC). Further particle identification information is provided by a time-of-propagation (TOP) counter, together with a ring imaging Cherenkov (ARICH) detector. Photon and electron reconstruction is provided by the CsI(Tl) electromagnetic calorimeter (ECL). Outside the superconducting solenoid  $K_L^0$  and muon, reconstruction is provided by an alternating sandwich structure of resistive plate chambers and iron absorbers (KLM), which also serves as magnetic flux returns for the solenoid.

Experimentally, the Belle II experiment profits from the clean  $e^+e^-$  environment and the known kinematics of the initial state, which allows it to reconstruct the energy difference  $\Delta E$  between the reconstructed energy and half  $\sqrt{s}$ , as well as the beam-energy substituted mass  $m_{ES}$ . These observables can significantly improve the signal-over-background ratios. The production of  $B\bar{B}$  meson pairs via the  $\Upsilon(4S)$  resonance furthermore allows full reconstruction of one of the B-mesons (B-tagging) using a full event interpretation. This allows for a particularly clean reconstruction of the other (signal) B-meson at the cost of a lower efficiency.

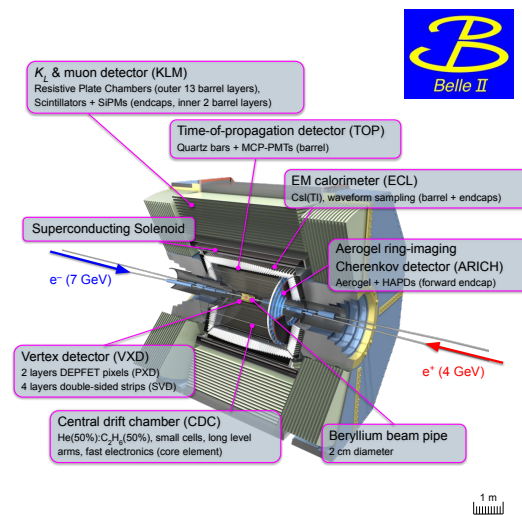


**Figure 4.** The Belle II detector at SuperKEKB. Figure taken from Ref. [38].

### 2.5. LHCb

The LHCb experiment, located at the Large Hadron Collider (LHC) at CERN (Geneva), is designed for precision measurements of  $b$ - and  $c$ -hadron decays [24]. The LHCb detector is designed as a single arm forward spectrometer covering the pseudorapidity range  $1.8 < \eta < 4.9$ . In the first two runs of data taking (Runs 1 and 2), LHCb collected data corresponding to an integrated luminosity of  $9 \text{ fb}^{-1}$ . After a major upgrade of the detector and trigger systems, LHCb is now taking its third run of data (Run 3) at a five-times larger instantaneous luminosity ( $2 \times 10^{33} \text{ cm}^2\text{s}^{-1}$ ). By the end of the LHC Run 4, LHCb expects to collect data corresponding to an integrated luminosity of  $50 \text{ fb}^{-1}$ .

A schematic view of the upgraded LHCb detector is shown in Figure 5. The primary  $pp$  interaction vertex is surrounded by a silicon vertex locator (VeLo), providing excellent impact parameter resolution. The tracking system further consists of a silicon strip detector (UT) before and a larger area scintillating fibre tracker (SciFi) after the magnet, which provides an integrated magnetic field of 4 Tm. The tracking system provides a relative momentum resolution  $\sigma(p)/p$  of up to 0.5%. Particle identification is provided by two ring-imaging Cherenkov (RICH) detectors, one located before and one after the magnet, and, in addition, the electromagnetic and hadronic calorimeters (ECAL and HCAL), as well as the muon chambers (M2–M5).

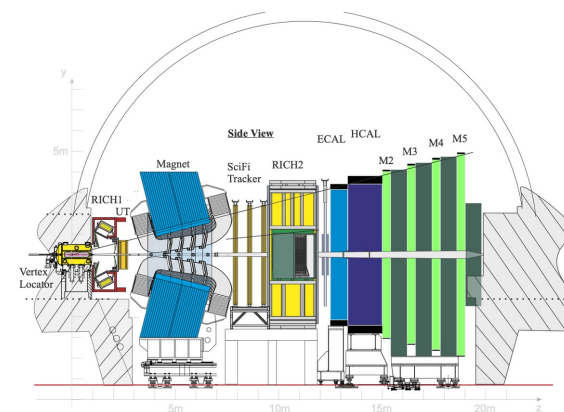


**Figure 5.** The upgraded LHCb detector. Figure taken from Ref. [26].

LHCb profits from enormous production cross sections at the LHC: during the LHC Run 2 at  $\sqrt{s} = 13 \text{ TeV}$ , LHCb measured cross sections of  $(154 \pm 14) \mu\text{b}^{-1}$  and  $(2940 \pm 241) \mu\text{b}^{-1}$  in the LHCb acceptance for beauty and charm quark productions, re-

spectively [39,40]. This results in enormous data samples of  $b$ - and  $c$ -hadrons, and, via their semileptonic decays, also  $\tau$ -leptons (e.g., from the decay  $D_s^+ \rightarrow \tau^+ \nu_\tau$ ). LHCb exploits these large samples to provide world-leading sensitivities for decays involving muons and electrons in the final state. The reconstruction of final states involving  $\tau$ -leptons is more challenging, but LHCb can exploit its excellent vertex resolution in kinematic fits. Following Run 4, the LHCb collaboration plans to perform a further upgrade of the detector, with a target luminosity of  $300 \text{ fb}^{-1}$  [41].

## 2.6. ATLAS and CMS

ATLAS and CMS are the two general purpose detectors of the LHC [29,30]. During the LHC Runs 1–2, ATLAS and CMS ran at instantaneous luminosities of up to  $2 \times 10^{34} \text{ cm}^{-2} \text{ s}^{-1}$ , twice the design luminosity of  $1 \times 10^{34} \text{ cm}^{-2} \text{ s}^{-1}$ . Both ATLAS and CMS collected data samples corresponding to an integrated luminosity of approximately  $165 \text{ fb}^{-1}$  during the LHC Runs 1–2. For Run 3, the target integrated luminosity is  $250 \text{ fb}^{-1}$ . Due to the large pile-up, the triggers at ATLAS and CMS are particularly optimized for high  $p_T$  signatures. ATLAS and CMS therefore provide world-leading sensitivities to lepton-flavour violating decays of the heavy  $Z$  and Higgs bosons. During the HL-LHC, the instantaneous luminosity will increase to up to  $7.5 \times 10^{34} \text{ cm}^{-2} \text{ s}^{-1}$ , and ATLAS and CMS expect to collect data samples corresponding to  $3 \text{ ab}^{-1}$  until the end of Run 6 [42,43].

## 3. Lepton-Flavour Violation in Purely Leptonic Decays

### 3.1. Muon Decays

#### 3.1.1. $\mu^+ \rightarrow e^+ \gamma$

As detailed in Section 2.1, searches for the decay  $\mu^+ \rightarrow e^+ \gamma$  are typically performed by stopping a positive muon beam in a target and looking for coincident mono-energetic positrons and photons with an energy of  $m_\mu/2$ , each in a back-to-back configuration. The sensitivity of experiments is limited by the ability to reject backgrounds, primarily from radiative muon decays (RMD)  $\mu^+ \rightarrow e^+ \bar{\nu}_\mu \nu_e \gamma$ , where the two neutrinos are carrying away a small fraction of the available energy, and from accidental coincidence of a positron and a photon from different processes. For the suppression of these backgrounds, the reconstructed positron and photon energies ( $E_+$  and  $E_\gamma$ ), the relative time of positron and photon,  $t_{e+\gamma} = t_\gamma - t_{e^+}$  calculated at the target, and the relative azimuthal and polar angles ( $\theta_{e+\gamma}$  and  $\phi_{e+\gamma}$ ) can be used. The currently most sensitive search has been performed by the MEG collaboration with the full data set taken during the years 2009–2013 [31]. The resulting events are shown in Figure 6 (left), where a cut on  $\cos \Theta_{e+\gamma} < -0.99963$ , where  $\Theta_{e+\gamma}$  is the relative stereo angle and  $|t_{e+\gamma}| < 0.24 \text{ ns}$  is applied. No statistically significant excess of events is observed in the signal region (denoted in blue); the best fit of the signal component yields a negative branching ratio, as shown in Figure 6 (right). As a result, the MEG collaboration sets a limit and finds  $\mathcal{B}(\mu^+ \rightarrow e^+ \gamma) < 4.2 \times 10^{-13}$  set by the MEG experiment at 90% confidence level (CL) [31], which constitutes the most stringent limit on this decay to date.

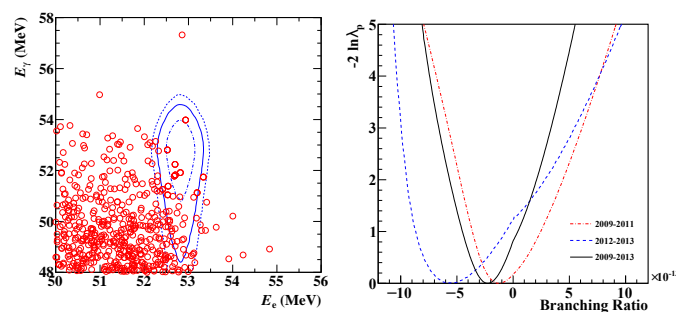


**Figure 6.** (Left) Event distribution in the  $(E_{e^+}, E_\gamma)$  plane. A cut on  $\cos \Theta_{e+\gamma} < -0.99963$  and  $|t_{e+\gamma}| < 0.24 \text{ ns}$  is applied. (Right) Resulting negative-log likelihood as function of the branching ratio. Figures taken from Ref. [31].

### 3.1.2. $\mu^+ \rightarrow e^+e^-e^+$

The search for the lepton-flavour violating decay  $\mu^+ \rightarrow e^+e^-e^+$  is complementary to the search for the decay  $\mu^+ \rightarrow e^+\gamma$ . The main background source for the signal channel is the RMD  $\mu^+ \rightarrow e^+e^-e^+\bar{\nu}_\mu\nu_e$ , where the photon is virtual and converts into an  $e^+e^-$  pair, and the two neutrinos are low energetic. Another relevant source of background arises from the accidental combination of an  $e^+e^-$  pair with low invariant mass and an uncorrelated positron. The most stringent limit on the branching fraction of the  $\mu^+ \rightarrow e^+e^-e^+$  decay is set by the SINDRUM experiment, described in Section 2.2 above. The SINDRUM experiment found no significant signal excess and set an upper limit of  $\mathcal{B}(\mu^+ \rightarrow e^+e^-e^+) < 1 \times 10^{-12}$  at 90% CL [15].

The Mu3e experiment [33], currently under construction at PSI, is aimed at reaching a sensitivity of  $10^{-16}$  to the  $\mu^+ \rightarrow e^+e^-e^+$  decay, four orders of magnitude lower than the limit set by the SINDRUM collaboration.

### 3.1.3. $\mu^-N \rightarrow e^-N$

The search for the lepton-flavour violating conversion process  $\mu^-N \rightarrow e^-N$  is performed by looking for the emission of an electron with an energy of  $E_{\mu e} = m_\mu c^2 - B_\mu - R$ , where  $B_\mu$  denotes the muon binding energy and  $R$  the atomic recoil, as discussed in Section 2.3. The dominant background contribution for these searches arises from muon decays in orbit, i.e.,  $\mu^- \rightarrow e^-\bar{\nu}_e\nu_\mu$ , that can mimic the signal if the two neutrinos carry very little energy. A second type of background originates from radiative pion capture that can arise if the beam exhibits a significant pion contamination. The SINDRUM II experiment suppresses these backgrounds by keeping the muon beam extremely clean through the use of a CH<sub>2</sub> moderator. Residual pion induced backgrounds can be removed through angular selection criteria. Figure 7 (top) shows the momentum distribution of events from a search for  $\mu-e$  conversion in gold, for which pion induced backgrounds have been removed. The data are in good agreement with the background-only hypothesis. Limits on  $\mu^-N \rightarrow e^-N$  processes are expressed as a ratio between the  $\mu-e$  conversion and the nuclear capture rates:

$$R_{\mu e} = \frac{\mu^-N \rightarrow e^-N}{\mu^-N \rightarrow \text{all muon captures}} \quad (1)$$

The SINDRUM II experiment has set the most stringent constraints on  $\mu-e$  conversion, resulting in upper limits of  $R_{\mu e} < 7 \times 10^{-13}$ ,  $R_{\mu e} < 8.9 \times 10^{-11}$  and  $R_{\mu e} < 4.6 \times 10^{-11}$  at 90% CL, using gold, titanium, and lead [16,44,45].

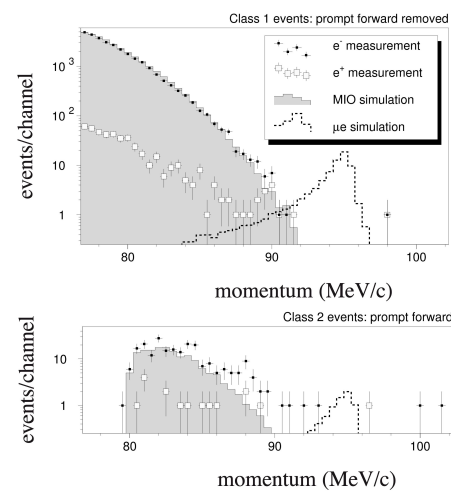


**Figure 7. (Top)** Comparison between the measured distribution and simulated muon decay-in-orbit events. In addition, the simulated shape of a potential lepton-flavour violating signal is given. For these events, contamination from pion-induced backgrounds are removed. **(Bottom)** Sample enriched with pion-induced backgrounds. Figure taken from Ref. [46].

The Mu2e [19], COMET [20], and DeeMe [21] experiments expect to improve on these limits for  $\mu$ - $e$  conversion and aim to reach sensitivities of  $\mathcal{O}(10^{-17})$ ,  $\mathcal{O}(10^{-17})$ , and  $\mathcal{O}(10^{-14})$ , respectively.

### 3.2. Tau Decays

Due to the large  $\tau$  mass, the branching fractions predicted by NP models for LFV  $\tau$  decays can be orders of magnitude larger than LFV  $\mu$  decays [47,48]. Moreover, their larger mass allows for a larger variety of final states, including neutrinoless semileptonic decays such as  $\tau^- \rightarrow \ell^- \pi^0$  and  $\tau^- \rightarrow \ell^- \pi^+ \pi^-$ . Despite being theoretically appealing, LFV  $\tau$  decays are more challenging from the experimental side. In contrast to muons, which can be manipulated and accelerated in beams, tau leptons have a significantly shorter lifetime ( $2.9 \times 10^{-13}$  s instead of  $2.2 \times 10^{-6}$  s) and can only be studied via their decay products.

As of today, most of the upper limits on the branching fractions of LFV  $\tau$  decays have been obtained by the BaBar and Belle experiments. At the LHC, searches for LFV  $\tau$  decays are feasible thanks to the large  $\tau$  production cross section. So far, the LHCb, ATLAS, and CMS experiments have produced upper limits for the  $\tau^- \rightarrow \mu^- \mu^+ \mu^-$  decay and LHCb also for the  $\tau^- \rightarrow p \mu^- \mu^-$  and  $\tau^- \rightarrow \bar{p} \mu^- \mu^+$  decays [49]. An overview of the current status of the observed upper limits on the branching fractions of LFV  $\tau$  decays is reported in Figure 8.

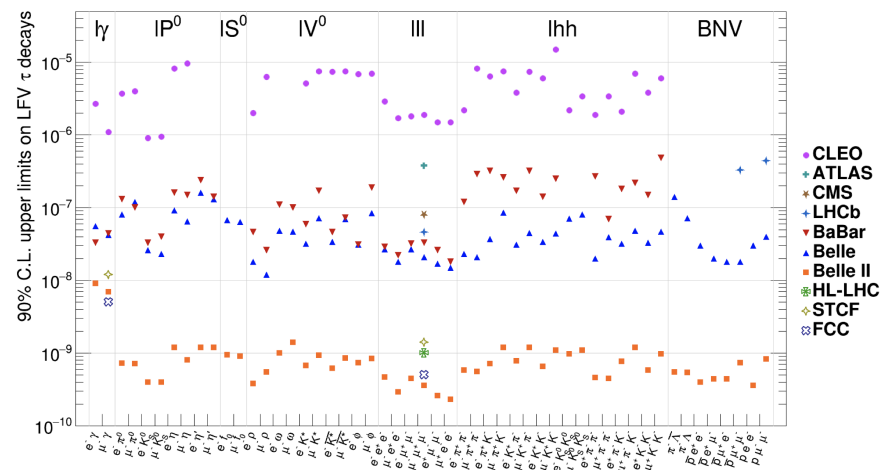


**Figure 8.** Current status of the observed upper limits on LFV  $\tau$  decays at CLEO, BaBar, Belle, LHCb, ATLAS, and CMS. In addition, projections for Belle II are reported. Figure taken from Ref. [50].

#### 3.2.1. $\tau^- \rightarrow \ell^- \gamma$

In many NP models, the  $\tau^- \rightarrow \ell^- \gamma$  (with  $\ell = e, \mu$ ) is predicted to be the dominant decay mode among all possible LFV  $\tau$  processes, with a branching fraction close to the current experimental sensitivity [48,51,52]. At B-factories, both the energy and the mass of the  $\tau$  leptons produced in pairs in the  $e^+e^-$  collisions are well known. The LFV candidate is reconstructed by dividing the event into two hemispheres, the “signal-” and the “tag-” side, which are expected to contain the LFV and the SM decays, respectively. Each of the two hemispheres has a reconstructed energy  $E_\tau$  expected to be equal to  $\sqrt{s}/2$  and invariant mass equal to the  $\tau$  lepton mass  $m_\tau$ . The search for  $\tau^- \rightarrow \ell^- \gamma$  decays is challenging due to the presence of irreducible backgrounds coming from  $\tau^- \rightarrow \ell^- \bar{\nu}_\ell \nu_\tau$  decays and an external photon, from hadronic  $\tau$  decays where the pion is misidentified as an electron or muon and from di-muon events misidentified as  $\tau^+ \tau^-$  pairs. Both BaBar and Belle conducted searches for  $\tau^- \rightarrow \ell^- \gamma$  decays on  $516 \text{ fb}^{-1}$  and  $988 \text{ fb}^{-1}$  of recorded data, respectively [53,54]. In the BaBar analysis, signal candidates are selected by means of two kinematic variables: the energy difference  $\Delta E = E_\tau - \sqrt{s}/2$  and the beam energy-constrained  $\tau$  mass ( $m_{EC}$ ). In the two dimensional plane of  $m_{EC}$  versus  $\Delta E$ , signal candidates are expected to be centred at  $(m_\tau, 0)$ . Belle, instead, examined the signal candidates in the  $\Delta E/\sqrt{s}$  versus  $M_{bc}$  plane,

$\Delta E/\sqrt{s}$  being the normalised energy difference and  $M_{bc}$  the beam-energy constrained invariant mass. In Figure 9, the 2D distribution of  $m_{EC}$  vs.  $\Delta E$  for  $\tau^- \rightarrow e^- \gamma$  candidates and of  $\Delta E/\sqrt{s}$  vs.  $M_{bc}$  for  $\tau^- \rightarrow \mu^- \gamma$  candidates is reported for the BaBar and Belle analysis, respectively.

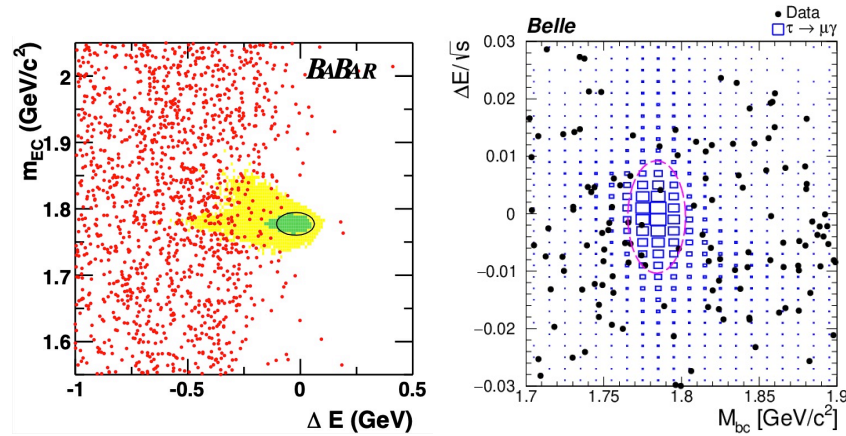


**Figure 9.** (Left)  $m_{EC}$  vs.  $\Delta E$  distribution for  $\tau^- \rightarrow e^- \gamma$  in the BaBar analysis [55]. (Right)  $\Delta E/\sqrt{s}$  vs.  $M_{bc}$  distribution for  $\tau^- \rightarrow \mu^- \gamma$  candidates in the Belle analysis [54].

Both experiments observed no significant excess of signal events, and the best upper limits of  $\mathcal{B}(\tau^- \rightarrow e^- \gamma) < 3.3 \times 10^{-8}$  (BaBar) and  $\mathcal{B}(\tau^- \rightarrow \mu^- \gamma) < 4.2 \times 10^{-8}$  (Belle) were set at 90% CL. Belle II is expected to improve the current sensitivity to the  $\tau^- \rightarrow \ell^- \gamma$  decay by one order of magnitude, thanks to a larger data set ( $50 \text{ ab}^{-1}$ ), higher signal efficiencies, and improved reconstruction and particle identification capabilities [56]. A comparable sensitivity is expected to be reached also at FCC-ee, the first stage of the Future Circular Colliders program [57].

### 3.2.2. $\tau^- \rightarrow \ell^- \ell^+ \ell^-$

Like  $\tau^- \rightarrow \ell^- \gamma$ , the  $\tau^- \rightarrow \ell^- \ell^+ \ell^-$  (with  $\ell = e, \mu$ ) decays also represent golden channels in the search for LFV  $\tau$  decays. Both at Babar and Belle, a search for all six possible final states, i.e.,  $e^- e^+ e^-$ ,  $\mu^- \mu^+ \mu^-$ ,  $\mu^- e^+ e^-$ ,  $\mu^- \mu^+ e^-$ ,  $e^- \mu^+ e^-$ ,  $\mu^- e^+ \mu^-$ , was conducted on  $468 \text{ fb}^{-1}$  and  $782 \text{ fb}^{-1}$  of data, respectively [58,59]. Signal candidates are selected by requiring the  $\tau$ -pair candidate to have four charged tracks with zero net charge, three in the “signal-” and one in the “tag-” side. The event selection, based on particle identification and kinematical requirements, is optimised mode by mode as each mode can be affected by a different mixture of backgrounds. In the Belle analysis, signal candidates are examined in the  $M_{3\ell}-\Delta E$  plane,  $M_{3\ell}$  being the  $\ell^- \ell^+ \ell^-$  invariant mass and  $\Delta E$  the difference between the summed energy and the beam energy in the centre-of-mass system. As an example, Figure 10 shows the events observed in the  $M_{3\ell}-\Delta E$  plane for the  $\tau^- \rightarrow e^- e^+ e^-$  and  $\tau^- \rightarrow \mu^- \mu^+ \mu^-$  modes. A similar approach is also adopted in the BaBar analysis. For all six modes, no signal events were observed in the signal region and upper limits were set on the branching fractions of  $\tau^- \rightarrow \ell^- \ell^+ \ell^-$  at 90% CL in the ranges  $(1.8\text{--}3.3) \times 10^{-8}$  (BaBar) and  $(1.5\text{--}2.7) \times 10^{-8}$  (Belle). The most stringent limits on the single modes, all set by Belle, are reported in Table 1.

At the LHC, the search for the  $\tau^- \rightarrow \mu^- \mu^+ \mu^-$  decay is feasible thanks to the clear signature provided by the muons in the final state. The strongest limit from a hadron collider on the branching fraction of the  $\tau^- \rightarrow \mu^- \mu^+ \mu^-$  decay is the one set by the LHCb experiment, where  $\tau$  leptons are mainly produced in  $D_s$ -meson decays. The largest source of background is the combinatorial one, arising from the random combination of charged tracks wrongly associated with the same vertex. Multivariate classification techniques based on kinematics and track quality information are used to suppress the combinatorial background, while particle identification information is exploited in the suppression of the background originating from hadron misidentification. A first search

was conducted on data collected in Run 1, corresponding to an integrated luminosity of  $\sim 3 \text{ fb}^{-1}$ . No significant excess of events was observed in the signal region and an upper limit of  $4.6 \times 10^{-8}$  was set at 90% CL [60]. The analysis on the Run 2 data set, corresponding to an integrated luminosity of  $\sim 6 \text{ fb}^{-1}$ , is currently ongoing. A search for the  $\tau^- \rightarrow \mu^- \mu^+ \mu^-$  decay was conducted by the ATLAS experiment on  $\tau$  leptons produced in  $W^- \rightarrow \tau^- \bar{\nu}_\tau$  decays; no signal event was observed and an upper limit of  $3.8 \times 10^{-8}$  was set at 90% CL [61]. The CMS collaboration recently published a new result for the upper limit on the branching fraction of  $\tau^- \rightarrow \mu^- \mu^+ \mu^-$ ,  $2.9 \times 10^{-8}$  at 90% CL, obtained on data collected in Run 2 and corresponding to an integrated luminosity of  $131 \text{ fb}^{-1}$  [62]. In this case,  $\tau$  leptons coming from both heavy-flavour hadron and  $W$  boson decays are exploited in the analysis. As also shown in Figure 8, Belle II is expected to improve the current limit on the  $\tau^- \rightarrow \mu^- \mu^+ \mu^-$  decay down to  $\mathcal{O}(10^{-9}\text{--}10^{-10})$ , with  $50 \text{ fb}^{-1}$  of collected data [56]. In the HL-LHC era, the LHCb experiment plans to reach a sensitivity of  $\mathcal{O}(10^{-9})$ , either confirming any Belle II discovery or contributing to a significant improvement of the combined limit [63]. A similar sensitivity is also expected from the ATLAS experiment, which plans to collect  $3 \text{ ab}^{-1}$  of data at 14 TeV during the HL-LHC campaign [64].

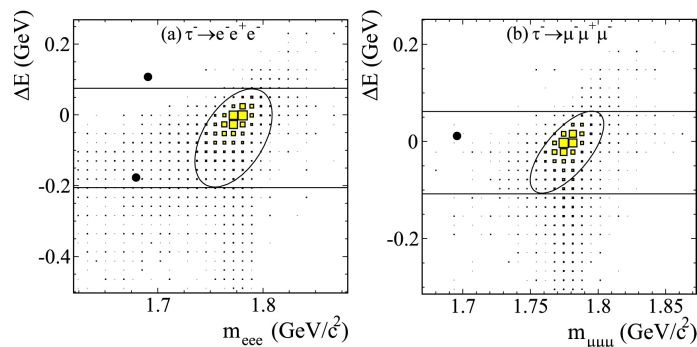


**Figure 10.** Scatter-plots for data (solid circles) and signal MC (filled boxes) over the  $\pm 20\sigma$  area in the  $M_{3\ell} - \Delta E$  plane for the  $\tau^- \rightarrow e^- e^+ e^-$  (a) and  $\tau^- \rightarrow \mu^- \mu^+ \mu^-$  (b) decays. The elliptical solid curve indicates the signal region, while the box inside the horizontal lines but excluding the elliptical region are used to estimate the background contamination in the signal region. Figure taken from Refs. [55].

## 4. Lepton-Flavour Violation in Hadron Decays

### 4.1. Lepton-Flavour Violating $b$ -Hadron Decays

#### 4.1.1. Final States Including Light Leptons

New Physics models, including leptoquark models and models including new heavy gauge bosons, can predict sizeable branching fractions for lepton-flavour violating  $b$ -hadron decays [65–69]. Searches for lepton-flavour violating  $b$ -hadron decays have been performed by LHCb and the B-factories. In searches for decays to final states with light leptons (i.e., electrons and muons) that include only charged tracks, the LHCb collaboration provides the most stringent limits. A search for the purely leptonic decays  $B_s^0 \rightarrow \mu^\pm e^\mp$  and  $B^0 \rightarrow \mu^\pm e^\mp$  was performed using the LHCb Run 1 data sample, corresponding to an integrated luminosity of  $3 \text{ fb}^{-1}$ . As evident from Figure 11, no signal was observed and exclusion limits of  $\mathcal{B}(B_s^0 \rightarrow \mu^\pm e^\mp) < 5.4 \times 10^{-9}$  and  $\mathcal{B}(B^0 \rightarrow \mu^\pm e^\mp) < 1.0 \times 10^{-9}$  at 90% CL were set [70]. The most stringent limits on semileptonic  $b \rightarrow s \mu^\pm e^\mp$  transitions have also been determined by the LHCb collaboration. Figure 12 shows signal candidates for the lepton-flavour violating decays  $B^0 \rightarrow K^{*0} \mu^+ e^-$  and  $B^0 \rightarrow K^{*0} \mu^- e^+$  using LHCb data corresponding to an integrated luminosity of  $9 \text{ fb}^{-1}$ . No significant signal is observed and LHCb sets limits of  $\mathcal{B}(B^0 \rightarrow K^{*0} \mu^+ e^-) < 5.7 \times 10^{-9}$ ,  $\mathcal{B}(B^0 \rightarrow K^{*0} \mu^- e^+) < 6.8 \times 10^{-9}$ , and  $\mathcal{B}(B_s^0 \rightarrow \phi \mu^\pm e^\mp) < 16.0 \times 10^{-9}$  at 90% CL [71]. For the decay  $B^+ \rightarrow K^+ \mu^\pm e^\mp$ , LHCb sets the limits of  $\mathcal{B}(B^+ \rightarrow K^+ \mu^+ e^-) < 6.4 \times 10^{-9}$  and  $\mathcal{B}(B^+ \rightarrow K^+ \mu^- e^+) < 7.0 \times 10^{-9}$  at 90% CL using  $3 \text{ fb}^{-1}$  of data [72]. The Babar and Belle collaborations have established the most stringent limits on the decays  $B^+ \rightarrow K^{*+} \mu^\pm e^\mp$  and  $B^0 \rightarrow K^0 \mu^\pm e^\mp$  at  $\mathcal{B}(B^+ \rightarrow K^{*+} \mu^\pm e^\mp) < 1.4 \times 10^{-6}$  and  $\mathcal{B}(B^0 \rightarrow K^0 \mu^\pm e^\mp) < 3.8 \times 10^{-8}$  (both at 90% CL), respectively [73,74]. The

best limit on the  $b \rightarrow d\mu^\pm e^\mp$  decay  $B \rightarrow \pi\mu^\pm e^\mp$  (isospin-averaged) of  $\mathcal{B}(B \rightarrow \pi\mu^\pm e^\mp) < 9.2 \times 10^{-8}$  at 90% CL has been established by the BaBar collaboration [75].

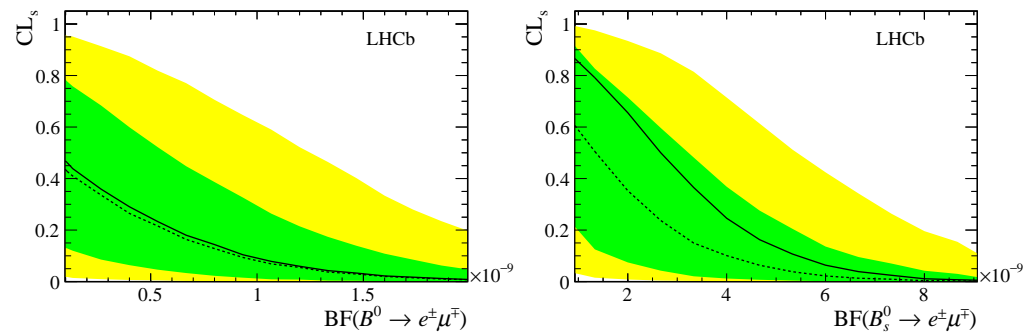


**Figure 11.** Limits for the decays (left)  $B^0 \rightarrow \mu^\pm e^\mp$  and (right)  $B_s^0 \rightarrow \mu^\pm e^\mp$  by the LHCb collaboration. Figure taken from Ref. [70].

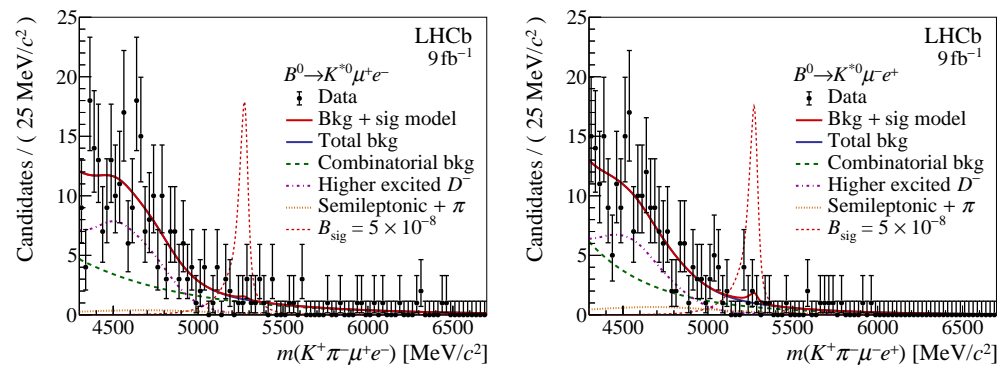


**Figure 12.** Signal candidates for the lepton-flavour violating decays (left)  $B^0 \rightarrow K^{*0}\mu^+e^-$  and (right)  $B^0 \rightarrow K^{*0}\mu^-e^+$  overlaid with fit projections. Figure taken from Ref. [71].

#### 4.1.2. Final States Including $\tau$ Leptons

Lepton-flavour violating decays of  $b$ -hadrons to final states including  $\tau$ -leptons are more challenging to reconstruct, especially at hadron colliders, where the kinematics of the initial state are not known. Nevertheless, the LHCb collaboration is able to leverage its precision tracking system to reconstruct the mass of the signal  $b$ -hadron using kinematic fits. Using the decay  $\tau^- \rightarrow \pi^- \pi^+ \pi^- (\pi^0) \nu_\tau$ , the LHCb collaboration sets the current best limits on the purely leptonic decays  $B^0 \rightarrow \tau^\pm \mu^\mp$  and  $B_s^0 \rightarrow \tau^\pm \mu^\mp$  using Run 1 data corresponding to an integrated luminosity of  $3 \text{ fb}^{-1}$ . Figure 13 (left) illustrates that the  $B_{(s)}^0$  meson masses can be well reconstructed despite the missing neutrino, which allows for a good separation of potential signals from background events. The search is performed in several bins of a BDT classifier output with increasing signal-over-background ratio. The most sensitive BDT bin is shown in Figure 13 (right). No signal is observed and LHCb sets limits of  $\mathcal{B}(B^0 \rightarrow \tau^\pm \mu^\mp) < 1.4 \times 10^{-5}$  and  $\mathcal{B}(B_s^0 \rightarrow \tau^\pm \mu^\mp) < 4.2 \times 10^{-5}$  at 90% CL [76]. Slightly less stringent limits on  $B^0 \rightarrow \tau^\pm \mu^\mp$  are provided by the BaBar and Belle collaborations [77,78]. These collaborations, however, have set the most stringent limits on the decay  $B^0 \rightarrow \tau^\pm e^\mp$  of  $\mathcal{B}(B^0 \rightarrow \tau^\pm e^\mp) < 2.8 \times 10^{-5}$  and  $\mathcal{B}(B^0 \rightarrow \tau^\pm e^\mp) < 1.6 \times 10^{-5}$  at 90% CL, respectively [77,78]. Semileptonic  $b \rightarrow s\tau^\pm \mu^\mp$  transitions have been searched for by LHCb, resulting in limits of  $\mathcal{B}(B^0 \rightarrow K^{*0}\tau^+\mu^-) < 1.0 \times 10^{-5}$  and  $\mathcal{B}(B^0 \rightarrow K^{*0}\tau^-\mu^+) < 8.2 \times 10^{-6}$  at 90% CL [79]. Using  $B_{s2}^0 \rightarrow B^+K^-$  decays, LHCb furthermore has set an upper limit of  $\mathcal{B}(B^+ \rightarrow K^+\mu^-\tau^+) < 3.9 \times 10^{-5}$ , also at 90% CL [80]. The most stringent limits on semileptonic  $b \rightarrow s\tau^\pm e^\mp$  transitions are provided by the BaBar collaboration, which provides the exclusion limits  $\mathcal{B}(B \rightarrow K\tau^+e^-) < 1.5 \times 10^{-5}$  and  $\mathcal{B}(B \rightarrow K\tau^-e^+) < 4.3 \times 10^{-5}$  at 90% CL [81]. A summary of the limits on lepton-flavour violating  $b$ -hadron decays is given in Table 1.

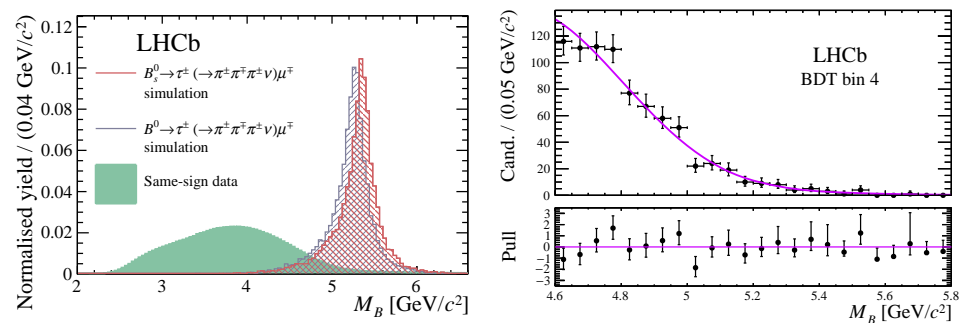


**Figure 13.** (Left) Reconstructed  $B$  mass for signal simulation and same-sign lepton data. (Right)  $B \rightarrow \tau^\pm \mu^\mp$  signal candidates in the most sensitive BDT bin. Figures taken from Ref. [76].

#### 4.2. Lepton-Flavour Violating $c$ -Hadron Decays

The most stringent limit on the purely leptonic decay  $D^0 \rightarrow \mu^\pm e^\mp$  has been set by the LHCb collaboration at  $\mathcal{B}(D^0 \rightarrow \mu^\pm e^\mp) < 1.3 \times 10^{-8}$  at 90% CL [82]. Concerning semileptonic lepton-flavour violating decays, LHCb provides leading limits for final states consisting of three charged tracks, resulting in  $\mathcal{B}(D^+ \rightarrow \pi^+ \mu^+ e^-) < 2.2 \times 10^{-7}$  and  $\mathcal{B}(D^+ \rightarrow \pi^+ \mu^- e^+) < 2.1 \times 10^{-7}$ , as well as  $\mathcal{B}(D^+ \rightarrow K^+ \mu^+ e^-) < 1.0 \times 10^{-7}$  and  $\mathcal{B}(D^+ \rightarrow K^+ \mu^- e^+) < 7.5 \times 10^{-8}$ , all set at 90% CL [83]. Slightly less stringent limits are also set for the corresponding  $D_s^+$  decays [83]. For limits on four-track modes the BaBar collaboration provides the most stringent limits. These include decays involving resonances where limits have been set on, e.g.,  $\mathcal{B}(D^0 \rightarrow \rho^0 \mu^\pm e^\mp) < 5.0 \times 10^{-7}$  and  $\mathcal{B}(D^0 \rightarrow \phi \mu^\pm e^\mp) < 5.1 \times 10^{-7}$ , as well as limits on inclusive final states such as  $\mathcal{B}(D^0 \rightarrow \pi^+ \pi^- \mu^\pm e^\mp) < 1.7 \times 10^{-6}$  and  $\mathcal{B}(D^0 \rightarrow K^+ K^- \mu^\pm e^\mp) < 1.0 \times 10^{-6}$ , all at 90% CL [84,85].

#### 4.3. Kaon Decays

Searches for LFV kaon decays have been performed for many years by various experiments, all leading to null results. The most stringent limit on the branching fraction of the  $K_L^0 \rightarrow \mu^\pm e^\mp$  decay belongs to the BNL collaboration, which produced a limit of  $\mathcal{B}(K_L^0 \rightarrow \mu^\pm e^\mp) < 4.7 \times 10^{-12}$  at 90% CL on data collected at the E871 experiment [27]. The KTeV experiment at Fermilab conducted searches for the lepton-flavour violating decays  $K_L^0 \rightarrow e^\pm e^\pm \mu^\mp \mu^\mp$ ,  $K_L^0 \rightarrow \pi^0 \mu^\pm e^\mp$  and  $K_L^0 \rightarrow \pi^0 \pi^0 \mu^\pm e^\mp$ , obtaining what are still today the most stringent limits on their branching fractions, i.e.,  $\mathcal{B}(K_L^0 \rightarrow e^\pm e^\pm \mu^\mp \mu^\mp) < 4.12 \times 10^{-11}$ ,  $\mathcal{B}(K_L^0 \rightarrow \pi^0 \mu^\pm e^\mp) < 7.56 \times 10^{-11}$ , and  $\mathcal{B}(K_L^0 \rightarrow \pi^0 \pi^0 \mu^\pm e^\mp) < 1.64 \times 10^{-10}$  at 90% CL [28,86]. Searches for LFV kaon decays have also been performed at the NA62 experiment at CERN, thanks to the large data set of kaon decays into lepton pairs collected between 2016 and 2018. In particular, a search for the  $K^+ \rightarrow \mu^- \nu e^+ e^+$  decay produced an upper limit of  $\mathcal{B}(K^+ \rightarrow \mu^- \nu e^+ e^+) < 8.1 \times 10^{-11}$  at 90% CL on the branching fraction of the decay. The result is obtained assuming a uniform phase space distribution of signal events and shows an improvement of a factor of 250 with respect to the previous limit [87]. The High-Intensity Kaon Experiments (HIKE) at CERN SPS, whose realisation is currently under discussion, plan to bring the sensitivity to LFV kaon decays down to  $\mathcal{O}(10^{-12})$  [88].

### 5. Lepton-Flavour Violation in Electroweak Boson Decays

#### 5.1. $Z \rightarrow \ell^\pm \ell'^\mp$ Decays

The most stringent limits on the branching fractions of  $Z \rightarrow \ell^\pm \ell'^\mp$  decays are set by the ATLAS experiment. The search for such decays is conducted by looking for an excess above the background contribution in the invariant mass distribution of the two leptons in correspondence of the  $Z$ -boson mass. For all three possible final states, the dominant background contribution comes from the lepton-flavour-conserving  $Z \rightarrow \tau^+ \tau^- \rightarrow \ell \ell' + 4\nu$  decay, where the two  $\tau$  leptons decay leptonically. The best limit on the  $Z \rightarrow e^\pm \mu^\mp$  decay,  $7.5 \times 10^{-7}$  at 95% CL, is based on data collected in  $pp$  collisions at a centre-of-mass energy of 8 TeV and corresponding to an integrated luminosity of  $20.3 \text{ fb}^{-1}$  [89]. The best limits

on the branching fraction of the  $Z \rightarrow e^\pm \tau^\mp$  and  $Z \rightarrow \mu^\pm \tau^\mp$  decays are derived from the combination of the results obtained in two different analyses. In the former, the search is conducted on events where the  $\tau$  lepton decays hadronically on  $159.3 \text{ fb}^{-1}$  of data from both Run 1 and Run 2 [90]. In the latter, only  $\tau$  leptons reconstructed via their leptonic decays are considered and  $139 \text{ fb}^{-1}$  of Run 2 data are used [91]. Both analyses make use of neural networks based on kinematic variables for the suppression of the background contamination. As an example, Figure 14 shows for the  $Z \rightarrow e^\pm \tau^\mp$  and  $Z \rightarrow \mu^\pm \tau^\mp$  channels the output of the neural networks for observed events as well as the predicted distributions for the main background contributions. Both analyses observed no significant excess of signal events, and the upper limits of  $5.0 \times 10^{-6}$  and  $6.5 \times 10^{-6}$  have been set at 95% CL on the  $Z \rightarrow e^\pm \tau^\mp$  and  $Z \rightarrow \mu^\pm \tau^\mp$  decays, respectively.

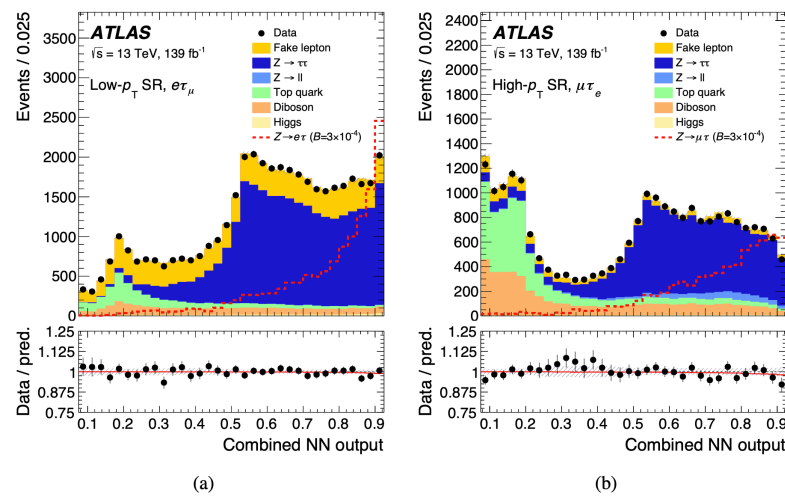


**Figure 14.** Distributions of the neural network output (a) for the low- $p_T$  signal region of the  $Z \rightarrow e^\pm \tau^\mp$  channel and (b) for the high- $p_T$  signal region of the  $Z \rightarrow \mu^\pm \tau^\mp$  channel. The expected signal (red dashed line) is shown normalised to an arbitrary  $\mathcal{B}(Z \rightarrow \ell\tau) = 3 \times 10^{-4}$  for visualization purposes. Figure taken from Ref. [91].

### 5.2. $H \rightarrow \ell^\pm \ell'^\mp$ Decays

Also for the  $H \rightarrow e^\pm \mu^\mp$  decay, the best limit is provided by the ATLAS experiment. The analysis is conducted on  $139 \text{ fb}^{-1}$  of data collected in  $pp$  collisions at  $\sqrt{s} = 13 \text{ TeV}$ . Similarly to what is described in the previous section, a narrow peak is searched for in the invariant mass distribution of the two leptons in correspondence of the Higgs boson mass. The background from top quarks is suppressed by identifying  $b$ -hadrons and neutrinos in the final state. As also shown in Figure 15, no evidence of the signal decay is found and an upper limit of  $\mathcal{B}(H \rightarrow e^\pm \mu^\mp) < 6.2 \times 10^{-5}$  is set at 95% CL [92].

The CMS experiment conducted a search for the  $H \rightarrow e^\pm \tau^\mp$  and  $H \rightarrow \mu^\pm \tau^\mp$  decays on  $137 \text{ fb}^{-1}$  of data collected in  $pp$  collisions happening at  $\sqrt{s} = 13 \text{ TeV}$ . The dominant background contributions to the signal decays come from  $Z \rightarrow \tau^+ \tau^-$  processes and from the misidentification of leptons. However, when the  $\tau$  is reconstructed via its leptonic decay, events from  $t\bar{t}$  processes can also contribute and have to be taken into account. The analysis makes use of boosted decision trees to discriminate between signal and background events, and a maximum likelihood fit to the output of the classifier is performed to extrapolate the final results. The observed data are in agreement with the background-only hypothesis, hence the upper limits of  $\mathcal{B}(H \rightarrow e^\pm \tau^\mp) < 0.22\%$  and  $\mathcal{B}(H \rightarrow \mu^\pm \tau^\mp) < 0.15\%$  are set at 95% CL [93]. The result for the  $H \rightarrow e^\pm \tau^\mp$  decay has been superseded by the one obtained in a more recent analysis conducted by the ATLAS collaboration on  $138 \text{ fb}^{-1}$  of data collected in  $pp$  collisions at  $\sqrt{s} = 13 \text{ TeV}$ . No significant excess of signal events is observed and upper limits are set on the branching fractions of the decays, i.e.,  $\mathcal{B}(H \rightarrow e^\pm \tau^\mp) < 0.20\%$  and  $\mathcal{B}(H \rightarrow \mu^\pm \tau^\mp) < 0.18\%$  [94].

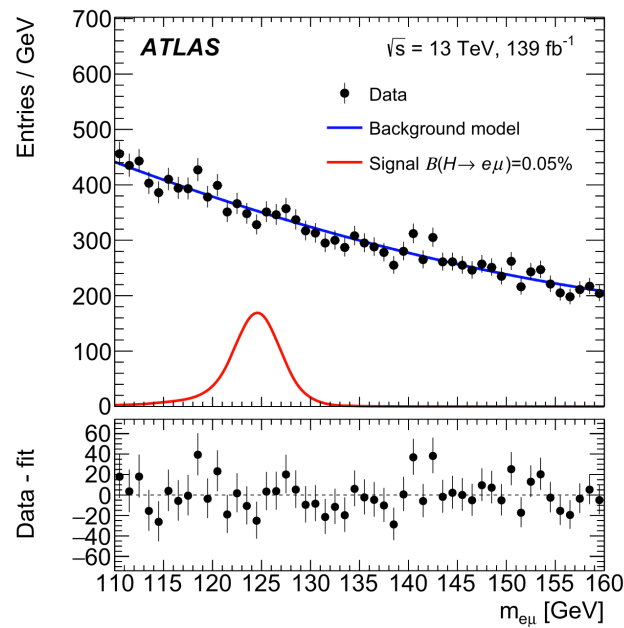


**Figure 15.** Comparison between the invariant mass distribution observed for the  $e^\pm\mu^\mp$  channel and the background-only model. The signal parameterisation obtained assuming  $B(H \rightarrow e^\pm\mu^\mp) = 0.05\%$  is also shown. Figure taken from Ref. [92].

## 6. Summary and Conclusions

We have presented an overview of searches for lepton-flavour violating processes in decays of leptons, hadrons, and heavy bosons. Due to space constraints, we were not able to cover all searches being performed, e.g., we did not discuss decays of light hadrons, charmonia, and quarkonia. A summary of some of the most stringent constraints for lepton-flavour violating processes is given in Table 1. No positive signal for lepton-flavour violation in the charged sector has been observed to date; however, many experiments are currently planned, under construction, or already running that aim to improve the present limits by often several orders of magnitude. These searches will either result in exciting signs of New Physics or set even stronger constraints on SM extensions.

**Table 1.** Summary table of the most stringent limits on a selection of lepton-flavour violating processes.

Process	Limit	CL	Experiment	Ref.
$\mu^+ \rightarrow e^+\gamma$	$4.3 \times 10^{-13}$	90%	MEG	[31]
$\mu^+ \rightarrow e^+e^-e^+$	$1.0 \times 10^{-12}$	90%	SINDRUM	[15]
$\mu^- \text{Ti} \rightarrow e^- \text{Ca}^*$	$8.9 \times 10^{-11}$	90%	SINDRUM II	[44]
$\mu^- \text{Pb} \rightarrow e^- \text{Pb}$	$4.6 \times 10^{-11}$	90%	SINDRUM II	[45]
$\mu^- \text{Au} \rightarrow e^- \text{Au}$	$7 \times 10^{-13}$	90%	SINDRUM II	[16]
$\tau^- \rightarrow e^- \gamma$	$3.3 \times 10^{-8}$	90%	BaBar	[53]
$\tau^- \rightarrow \mu^- \gamma$	$4.2 \times 10^{-8}$	90%	Belle	[54]
$\tau^- \rightarrow e^- e^+ e^-$	$2.7 \times 10^{-8}$	90%	Belle	[59]
$\tau^- \rightarrow \mu^- \mu^+ \mu^-$	$2.1 \times 10^{-8}$	90%	Belle	[59]
$\tau^- \rightarrow \mu^- e^+ e^-$	$1.8 \times 10^{-8}$	90%	Belle	[59]
$\tau^- \rightarrow \mu^- \mu^+ e^-$	$2.7 \times 10^{-8}$	90%	Belle	[59]
$\tau^- \rightarrow e^- \mu^+ e^-$	$1.5 \times 10^{-8}$	90%	Belle	[59]
$\tau^- \rightarrow \mu^- e^+ \mu^-$	$1.7 \times 10^{-8}$	90%	Belle	[59]

Table 1. Cont.

Process	Limit	CL	Experiment	Ref.
$B^0 \rightarrow \mu^\pm e^\mp$	$1.0 \times 10^{-9}$	90%	LHCb	[70]
$B_s^0 \rightarrow \mu^\pm e^\mp$	$5.4 \times 10^{-9}$	90%	LHCb	[70]
$B^0 \rightarrow K^{*0} \mu^+ e^-$	$5.7 \times 10^{-9}$	90%	LHCb	[71]
$B^0 \rightarrow K^{*0} \mu^- e^+$	$6.8 \times 10^{-9}$	90%	LHCb	[71]
$B_s^0 \rightarrow \phi \mu^\pm e^\mp$	$1.6 \times 10^{-8}$	90%	LHCb	[71]
$B^+ \rightarrow K^+ \mu^+ e^-$	$6.4 \times 10^{-9}$	90%	LHCb	[72]
$B^+ \rightarrow K^+ \mu^- e^+$	$7.0 \times 10^{-9}$	90%	LHCb	[72]
$B^0 \rightarrow \tau^\pm \mu^\mp$	$1.5 \times 10^{-5}$	90%	LHCb	[76]
$B_s^0 \rightarrow \tau^\pm \mu^\mp$	$4.2 \times 10^{-5}$	90%	LHCb	[76]
$B^0 \rightarrow \tau^\pm e^\mp$	$1.6 \times 10^{-5}$	90%	Belle	[78]
$B^0 \rightarrow K^{*0} \tau^+ \mu^-$	$1.0 \times 10^{-5}$	90%	LHCb	[79]
$B^0 \rightarrow K^{*0} \tau^- \mu^+$	$8.2 \times 10^{-6}$	90%	LHCb	[79]
$D^0 \rightarrow \mu^\pm e^\mp$	$1.3 \times 10^{-8}$	90%	LHCb	[82]
$D^+ \rightarrow \pi^+ \mu^+ e^-$	$2.2 \times 10^{-7}$	90%	LHCb	[83]
$D^+ \rightarrow \pi^+ \mu^- e^+$	$2.1 \times 10^{-7}$	90%	LHCb	[83]
$D^+ \rightarrow K^+ \mu^+ e^-$	$1.0 \times 10^{-7}$	90%	LHCb	[83]
$D^+ \rightarrow K^+ \mu^- e^+$	$7.5 \times 10^{-8}$	90%	LHCb	[83]
$K_L^0 \rightarrow \mu^\pm e^\mp$	$4.7 \times 10^{-12}$	90%	BNL	[27]
$K_L^0 \rightarrow e^\pm e^\pm \mu^\mp \mu^\mp$	$4.12 \times 10^{-11}$	90%	KTeV	[28]
$K_L^0 \rightarrow \pi^0 \mu^\pm e^\mp$	$7.56 \times 10^{-11}$	90%	KTeV	[86]
$K_L^0 \rightarrow \pi^0 \pi^0 \mu^\pm e^\mp$	$1.64 \times 10^{-10}$	90%	KTeV	[86]
$K^+ \rightarrow \mu^- \nu e^+ e^+$	$8.1 \times 10^{-11}$	90%	NA62	[87]
$Z \rightarrow e^\pm \mu^\mp$	$7.5 \times 10^{-7}$	95%	ATLAS	[89]
$Z \rightarrow e^\pm \tau^\mp$	$5.0 \times 10^{-6}$	95%	ATLAS	[91]
$Z \rightarrow \mu^\pm \tau^\mp$	$6.5 \times 10^{-6}$	95%	ATLAS	[91]
$H \rightarrow e^\pm \mu^\mp$	$6.2 \times 10^{-5}$	95%	ATLAS	[92]
$H \rightarrow e^\pm \tau^\mp$	$2.0 \times 10^{-3}$	95%	ATLAS	[94]
$H \rightarrow \mu^\pm \tau^\mp$	$1.5 \times 10^{-3}$	95%	CMS	[93]

**Author Contributions:** G.F. and C.L. contributed equally to this work. All authors have read and agreed to the published version of the manuscript.

**Funding:** Deutsche Forschungsgemeinschaft (DFG), grant identifiers LA 3937/1-1/2 and LA 3937/2-1.

**Acknowledgments:** C. L. gratefully acknowledges support by the Deutsche Forschungsgemeinschaft (DFG), grant identifiers LA 3937/1-1/2 and LA 3937/2-1.

**Conflicts of Interest:** The authors declare no conflicts of interest.

## References

- Fukuda, Y.; Hayakawa, T.; Ichihara, E.; Inoue, K.; Ishihara, K.; Ishino, H.; Itow, Y.; Kajita, T.; Kameda, J.; Kasuga, S.; et al. Evidence for oscillation of atmospheric neutrinos. *Phys. Rev. Lett.* **1998**, *81*, 1562–1567. [\[CrossRef\]](#)
- Ahmad, Q.R.; Allen, R.C.; Andersen, T.C.; Anglin, J.D.; Bühler, G.; Barton, J.C.; Beier, E.W.; Bercovitch, M.; Bigu, J.; Biller, S.; et al. Measurement of the rate of  $\nu_e + d \rightarrow p + p + e^-$  interactions produced by  $^8\text{B}$  solar neutrinos at the Sudbury Neutrino Observatory. *Phys. Rev. Lett.* **2001**, *87*, 071301. [\[CrossRef\]](#) [\[PubMed\]](#)
- Petcov, S.T. The Processes  $\mu \rightarrow e + \gamma$ ,  $\mu \rightarrow e + \bar{\nu}$ ,  $\nu' \rightarrow \nu + \gamma$  in the Weinberg-Salam Model with Neutrino Mixing. *Sov. J. Nucl. Phys.* **1977**, *25*, 340.
- Bilenky, S.M.; Petcov, S.T.; Pontecorvo, B. Lepton Mixing,  $\mu \rightarrow e\gamma$  Decay and Neutrino Oscillations. *Phys. Lett. B* **1977**, *67*, 309. [\[CrossRef\]](#)
- Marciano, W.J.; Sanda, A.I. Exotic Decays of the Muon and Heavy Leptons in Gauge Theories. *Phys. Lett. B* **1977**, *67*, 303–305. [\[CrossRef\]](#)
- Lee, B.W.; Pakvasa, S.; Shrock, R.E.; Sugawara, H. Muon and Electron Number Nonconservation in a V-A Gauge Model. *Phys. Rev. Lett.* **1977**, *38*, 937. [\[CrossRef\]](#)
- Lee, B.W.; Shrock, R.E. Natural Suppression of Symmetry Violation in Gauge Theories: Muon—Lepton and Electron Lepton Number Nonconservation. *Phys. Rev. D* **1977**, *16*, 1444. [\[CrossRef\]](#)
- Ardu, M.; Pezzullo, G. Introduction to Charged Lepton Flavor Violation. *Universe* **2022**, *8*, 299. [\[CrossRef\]](#)

9. Calibbi, L.; Signorelli, G. Charged Lepton Flavour Violation: An Experimental and Theoretical Introduction. *Riv. Nuovo Cim.* **2018**, *41*, 71–174. [[CrossRef](#)]
10. Bernstein, R.H.; Cooper, P.S. Charged Lepton Flavor Violation: An Experimenter's Guide. *Phys. Rept.* **2013**, *532*, 27–64. [[CrossRef](#)]
11. Hernandez Villanueva, M. Experimental review of Lepton Flavor Violation searches. In Proceedings of the 20th Conference on Flavor Physics and CP Violation, Oxford, MS, USA, 23–27 May 2022; Volume 8.
12. Mihara, S.; Miller, J.P.; Paradisi, P.; Piredda, G. Charged Lepton Flavor-Violation Experiments. *Ann. Rev. Nucl. Part. Sci.* **2013**, *63*, 531–552. [[CrossRef](#)]
13. Renga, F. Experimental searches for muon decays beyond the Standard Model. *Rev. Phys.* **2019**, *4*, 100029. [[CrossRef](#)]
14. Adam, J.; Bai, X.; Baldini, A.M.; Baracchini, E.; Bemporad, C.; Boca, G.; Cattaneo, P.W.; Cavoto, G.; Cei, F.; Cerri, C.; et al. The MEG detector for  $\mu^+ \rightarrow e^+ \gamma$  decay search. *Eur. Phys. J. C* **2013**, *73*, 2365. [[CrossRef](#)]
15. Bellgardt, U.; Otter, G.; Eichler, R.; Felawka, L.; Niebuhr, C.; Walter, H.K.; Bertl, W.; Lordong, N.; Martino, J.; Egli, S.; et al. Search for the Decay  $\mu^+ \rightarrow e^+ e^+ e^-$ . *Nucl. Phys. B* **1988**, *299*, 1–6. [[CrossRef](#)]
16. Bertl, W.H.; Engfer, R.; Hermes, E.A.; Kurz, G.; Kozlowski, T.; Kuth, J.; Otter, G.; Rosenbaum, F.; Ryskulov, N.M.; van der Schaaf, A.; et al. A Search for muon to electron conversion in muonic gold. *Eur. Phys. J. C* **2006**, *47*, 337–346. [[CrossRef](#)]
17. Baldini, A.M.; Baracchini, E.; Bemporad, C.; Berg, F.; Biasotti, M.; Boca, G.; Cattaneo, P.W.; Cavoto, G.; Cei, F.; Chiappini, M.; et al. The design of the MEG II experiment. *Eur. Phys. J. C* **2018**, *78*, 380. [[CrossRef](#)]
18. Arndt, K.; Augustin, H.; Baesso, P.; Berger, N.; Berg, F.; Betancourt, C.; Bortoletto, D.; Bravar, A.; Briggli, K.; vom Bruch, D.; et al. Technical design of the phase I Mu3e experiment. *Nucl. Instrum. Meth. A* **2021**, *1014*, 165679. [[CrossRef](#)]
19. Bartoszek, L.; Barnes, E.; Miller, J.P.; Mott, J.; Palladino, A.; Quirk, J.; Roberts, B.L.; Crnkovic, J.; Polychronakos, V.; Tishchenko, V.; et al. Mu2e Technical Design Report. Technical Report FERMILAB-DESIGN-2014-01. *arXiv* **2014**, arXiv:1501.05241.
20. Abramishvili, R.; Adamov, G.; Akhmetshin, R.R.; Allin, A.; Angélique, J.C.; Anishchik, V.; Aoki, M.; Aznabayev, D.; Bagaturia, I.; Ban, G.; et al. COMET Phase-I Technical Design Report. *PTEP* **2020**, *2020*, 033C01. [[CrossRef](#)]
21. Teshima, N. Status of the DeeMe Experiment, an Experimental Search for  $\mu$ -e Conversion at J-PARC MLF. *PoS* **2020**, *NuFact2019*, 082. [[CrossRef](#)]
22. Aubert, B.; Bazana, A.; Bouchama, A.; Boutignya, D.; De Bonisa, I.; Faviera, J.; Gaillarda, J.-M.; Jeremiea, A.; Karyotakisa, Y.; Le Flour, T.; et al. The BaBar detector. *Nucl. Instrum. Meth. A* **2002**, *479*, 1–116. [[CrossRef](#)]
23. Abashian, A.; Gotowa, K.; Morgana, N.; Piilonena, L.; Schrenka, S.; Abeb, K.; Adachib, I.; Alexanderb, J.P.; Aokib, K.; Beharib, S.; et al. The Belle Detector. *Nucl. Instrum. Meth. A* **2002**, *479*, 117–232. [[CrossRef](#)]
24. Alves, A.A., Jr.; Andrade Filho, L.M.; Barbosa, A.F.; Bediaga, I.; Cernicchiaro, G.; Guerrer, G.; Lima, H.P., Jr.; Machado, A.A.; Magnin, J.; Marujo, F.; et al. The LHCb Detector at the LHC. *JINST* **2008**, *3*, S08005. [[CrossRef](#)]
25. Abe, T.; Adachi, I.; Adamczyk, K.; Ahn, S.; Aihara, H.; Akai, K.; Alois, M.; Andricek, L.; Aoki, K.; Arai, Y.; et al. Belle II Technical Design Report. *arXiv* **2010**, arXiv:1011.0352.
26. Aaij, R.; Abdelmotteleb, A.S.W.; Abellan Beteta, C.; Abudinén, F.; Achard, C.; Ackernley, T.; Adeva, B.; Adinolfi, M.; Adlarson, P.; Afsharnia, H.; et al. The LHCb upgrade I. *arXiv* **2023**, arXiv:2305.10515.
27. Ambrose, D.; Arroyo, C.; Bachman, M.; Connor, D.; Eckhause, M.; Graessle, S.; Hancock, A. D.; Hartman, K.; Hebert, M.; Hoff, C.H.; et al. New limit on muon and electron lepton number violation from  $K_L^0 \rightarrow \mu^\pm e^\mp$  decay. *Phys. Rev. Lett.* **1998**, *81*, 5734–5737. [[CrossRef](#)]
28. Alavi-Harati, A.; Alexopoulos, T.; Arenton, M.; Arisaka, K.; Barbosa, R.F.; Barker, A.R.; Barrio, M.; Bellantoni, L.; Bellavance, A.; Blucher, E.; et al. Measurements of the Decay  $K_L \rightarrow e^+ e^- \mu^+ \mu^-$ . *Phys. Rev. Lett.* **2003**, *90*, 141801. [[CrossRef](#)] [[PubMed](#)]
29. Aad, G.; Abat, E.; Abdallah, J.; Abdelalim, A.A.; Abdesselam, A.; Abidinov, O.; Abi, B.A.; Abolins, M.; Abramowicz, H.; Acerbi, E.; et al. The ATLAS Experiment at the CERN Large Hadron Collider. *JINST* **2008**, *3*, S08003. [[CrossRef](#)]
30. Chatrchyan, S.; Hmayakyan, G.; Khachatryan, V.; Sirunyan, A.M.; Adam, W.; Bauer, T.; Bergauer, T.; Bergauer, H.; Dragicevic, M.; Erö, J.; et al. The CMS Experiment at the CERN LHC. *JINST* **2008**, *3*, S08004. [[CrossRef](#)]
31. Baldini, A.M.; Bao, Y.; Baracchini, E.; Bemporad, C.; Berg, F.; Biasotti, M.; Boca, G.; Cascella, M.; Cattaneo, P.W.; Cavoto, G.; et al. Search for the lepton flavour violating decay  $\mu^+ \rightarrow e^+ \gamma$  with the full dataset of the MEG experiment. *Eur. Phys. J. C* **2016**, *76*, 434. [[CrossRef](#)]
32. Afanaciev, K.; Baldini, A.M.; Ban, S.; Baranov, V.; Benmansour, H.; Biasotti, M.; Boca, G.; Cattaneo, P.W.; Cavoto, G.; Cei, F.; et al. A search for  $\mu^+ \rightarrow e^+ \gamma$  with the first dataset of the MEG II experiment. *Eur. Phys. J. C* **2024**, *84*, 216. [[CrossRef](#)]
33. Blondel, A.; Bravar, A.; Pohl, M.; Bachmann, S.; Berger, N.; Kiehn, M.; Schöning, A.; Wiedner, D.; Windelband, B.; Eckert, P.; et al. Research Proposal for an Experiment to Search for the Decay  $\mu \rightarrow eee$ . *arXiv* **2013**, arXiv:1301.6113.
34. Augustin, H.; Perić, I.; Schöning, A.; Weber, A. The MuPix sensor for the Mu3e experiment. *Nucl. Instrum. Meth. A* **2020**, *979*, 164441. [[CrossRef](#)]
35. Aiba, M.; Amato, A.; Antognini, A.; Ban, S.; Berger, N.; Caminada, L.; Chislett, R.; Crivelli, P.; Crivellin, A.; Dal Maso, G.; et al. Science Case for the new High-Intensity Muon Beams HIMB at PSI. *arXiv* **2021**, arXiv:2111.05788.
36. Van der Schaaf, A. SINDRUM II. *SciPost Phys. Proc.* **2021**, *5*, 008. [[CrossRef](#)]
37. Kou, E.; Urquijo, P.; Altmannshofer, W.; Beaujean, F.; Bell, G.; Beneke, M.; Bigi, I.I.; Bishara, F.; Blanke, M.; Bobeth, C.; et al. The Belle II Physics Book. *PTEP* **2019**, *2019*, 123C01. [[CrossRef](#)]

38. Natochii, A.; Browder, T.E.; Cao, L.; Cautero, G.; Dreyer, S.; Frey, A.; Gabrielli, A.; Giuressi, D.; Ishibashi, T.; Jin, Y.; et al. Measured and projected beam backgrounds in the Belle II experiment at the SuperKEKB collider. *Nucl. Instrum. Meth. A* **2023**, *1055*, 168550. [CrossRef]
39. Aaij, R.; Adeva, B.; Adinolfi, M.; Ajaltouni, Z.; Akar, S.; Albrecht, J.; Alessio, F.; Alexander, M.; Ali, S.; Alkhazov, G.; et al. Measurement of the  $b$ -quark production cross-section in 7 and 13 TeV  $pp$  collisions. *Phys. Rev. Lett.* **2017**, *118*, 052002. [CrossRef]
40. Aaij, R.; Abellán Beteta, C.; Adeva, B.; Adinolfi, M.; Affolder, A.; Ajaltouni, Z.; Akar, S.; Albrecht, J.; Alessio, F.; Alexander, M.; et al. Measurements of prompt charm production cross-sections in  $pp$  collisions at  $\sqrt{s} = 13$  TeV. *JHEP* **2016**, *3*, 159. [CrossRef]
41. Framework TDR for the LHCb Upgrade II: Opportunities in Flavour Physics, and Beyond, in the HL-LHC Era. 2021. Technical Report CERN-LHCC-2021-012, LHCb-TDR-023. 2021. Available online: <https://inspirehep.net/literature/2071542> (accessed on 1 February 2024).
42. Snowmass White Paper Contribution: Physics with the Phase-2 ATLAS and CMS Detectors. ATLAS Public Note ATL-PHYS-PUB-2022-018. 2022. Available online: <https://cds.cern.ch/record/2805993> (accessed on 1 February 2024).
43. The Phase-2 Upgrade of the CMS Muon Detectors. Technical Report CERN-LHCC-2017-012, CMS-TDR-016, CERN, Geneva. 2017. Available online: <https://cds.cern.ch/record/2283189> (accessed on 1 February 2024).
44. Dohmen, C.; Groth, K.-D.; Heer, B.; Honecker, W.; Otter, G.; Steinrücken, B.; Wintz, P.; Djordjadze, V.; Hofmann, J.; Kozłowski, T.; et al. Test of lepton flavor conservation in  $\mu \rightarrow e$  conversion on titanium. *Phys. Lett. B* **1993**, *317*, 631–636. [CrossRef]
45. Honecker, W.; Dohmen, C.; Haan, H.; Junker, D.; Otter, G.; Starlinger, M.; Wintz, P.; Hofmann, J.; Bertl, W.; Egger, J.; et al. Improved limit on the branching ratio of  $\mu \rightarrow e$  conversion on lead. *Phys. Rev. Lett.* **1996**, *76*, 200–203. [CrossRef]
46. Raidal, M.; van der Schaaf, A.; Bigi, I.; Mangano, M.L.; Semertzidis, Y.; Abel, S.; Albino, S.; Antusch, S.; Arganda, E.; Bajc, B.; et al. Flavour physics of leptons and dipole moments. *Eur. Phys. J. C* **2008**, *57*, 13–182. [CrossRef]
47. Arganda, E.; Herrero, M.J. Testing supersymmetry with lepton flavor violating  $\tau$  and  $\mu$  decays. *Phys. Rev. D* **2006**, *73*, 055003. [CrossRef]
48. Calibbi, L.; Faccia, A.; Masiero, A.; Vempati, S.K. Lepton flavour violation from SUSY-GUTs: Where do we stand for MEG, PRISM/PRIME and a super flavour factory. *Phys. Rev. D* **2006**, *74*, 116002. [CrossRef]
49. Aaij, R.; Abellán Beteta, C.; Adeva, B.; Adinolfi, M.; Adrover, C.; Affolder, A.; Ajaltouni, Z.; Albrecht, J.; Alessio, F.; Alexander, M.; et al. Searches for violation of lepton flavour and baryon number in tau lepton decays at LHCb. *Phys. Lett. B* **2013**, *724*, 36–45. [CrossRef]
50. Banerjee, S.; Cirigliano, V.; Dam, M.; Deshpande, A.; Fiorini, L.; Fuyuto, K.; Gal, C.; Husek, T.; Mereghetti, E.; Monsálvez-Pozo, K.; et al. Snowmass 2021 White Paper: Charged lepton flavor violation in the tau sector. *arXiv* **2022**, arXiv:2203.14919.
51. Brignole, A.; Rossi, A. Anatomy and phenomenology of mu-tau lepton flavor violation in the MSSM. *Nucl. Phys. B* **2004**, *701*, 3–53. [CrossRef]
52. Ellis, J.R.; Hisano, J.; Raidal, M.; Shimizu, Y. A New parametrization of the seesaw mechanism and applications in supersymmetric models. *Phys. Rev. D* **2002**, *66*, 115013. [CrossRef]
53. Aubert, B.; Karyotakis, Y.; Lees, J.P.; Poireau, V.; Prencipe, E.; Prudent, X.; Tisserand, V.; Garra Tico, J.; Grauges, E.; Martinelli, M.; et al. Searches for Lepton Flavor Violation in the Decays  $\tau^+ \rightarrow e^+ \gamma$  and  $\tau^+ \rightarrow \mu^+ \gamma$ . *Phys. Rev. Lett.* **2010**, *104*, 021802. [CrossRef]
54. Uno, K.; Hayasaka, K.; Inami, K.; Adachi, I.; Aihara, H.; Asner, D.M.; Atmacan, H.; Aushev, T.; Ayad, R.; Babu, V.; et al. Search for lepton-flavor-violating tau-lepton decays to  $\ell \gamma$  at Belle. *JHEP* **2021**, *10*, 19. [CrossRef]
55. Bevan, A.J.; Golob, B.; Mannel, T.H.; Prell, S.; Yabsley, B.D.; Aihara, H.; Anulli, F.; Arnaud, N.; Aushev, T.; Beneke, M.; et al. The Physics of the B Factories. *Eur. Phys. J. C* **2014**, *74*, 3026. [CrossRef]
56. Aggarwal, L.; Banerjee, S.; Bansal, S.; Bernlochner, F.; Bertemes, M.; Bhardwaj, V.; Bondar, A.; Browder, T.E.; Cao, L.; Campajola, M.; et al. Snowmass White Paper: Belle II physics reach and plans for the next decade and beyond. *arXiv* **2022**, arXiv:2207.06307.
57. Abada, A.; Abbrescia, M.; AbdusSalam, S.S.; Abdyukhanov, I.; Abelleira Fernandez, J.; Abramov, A.; Aburaia, M.; Acar, A.O.; Adzic, P.R.; Agrawal, P.; et al. FCC-ee: The Lepton Collider. *Eur. Phys. J. Spec. Top.* **2019**, *228*, 261–623. [CrossRef]
58. Lees, J.P.; Poireau, V.; Prencipe, E.; Tisserand, V.; Garra Tico, J.; Grauges, E.; Martinelli, M.; Palano, A.; Pappagallo, M.; Eigen, G.; et al. Limits on tau Lepton-Flavor Violating Decays in three charged leptons. *Phys. Rev. D* **2010**, *81*, 111101. [CrossRef]
59. Hayasaka, K.; Inami, K.; Miyazaki, Y.; Arinstein, K.; Aulchenko, V.; Aushev, T.; Bakich, A.M.; Bay, A.; Belous, K.; Bhardwaj, V.; et al. Search for Lepton Flavor Violating  $\tau$  Decays into Three Leptons with 719 Million Produced  $\tau^+ \tau^-$  Pairs. *Phys. Lett. B* **2010**, *687*, 139–143. [CrossRef]
60. Aaij, R.; Adeva, B.; Adinolfi, M.; Affolder, A.; Ajaltouni, Z.; Akar, S.; Albrecht, J.; Alessio, F.; Alexander, M.; Ali, S.; et al. Search for the lepton flavour violating decay  $\tau^- \rightarrow \mu^- \mu^+ \mu^-$ . *JHEP* **2015**, *2*, 121. [CrossRef]
61. Aad, G.; Abbott, B.; Abdallah, J.; Abdinov, O.; Aben, R.; Abolins, M.; AbouZeid, O.S.; Abramowicz, H.; Abreu, H.; Abreu, R.; et al. Probing lepton flavour violation via neutrinoless  $\tau \rightarrow 3\mu$  decays with the ATLAS detector. *Eur. Phys. J. C* **2016**, *76*, 232. [CrossRef]
62. Hayrapetyan, A.; Tumasyan, A.; Adam, W.; Andrejkovic, J.W.; Bergauer, T.; Chatterjee, S.; Damanakis, K.; Dragicevic, M.; Hussain, P.S.; Jeitler, M.; et al. Search for the lepton flavor violating  $\tau \rightarrow 3\mu$  decay in proton-proton collisions at  $\sqrt{s} = 13$  TeV. *arXiv* **2023**, arXiv:2312.02371.
63. Bediaga, I.; Cruz Torres, M.; De Miranda, J.M.; Gomes, A.; Massafferri, A.; Molina Rodriguez, J.; dos Reis, A.C.; Soares Lavra, I.; Tourinho Jadallah Aoude, R.; Amato, S.; et al. Physics case for an LHCb Upgrade II - Opportunities in flavour physics, and beyond, in the HL-LHC era. *arXiv* **2018**, arXiv:1808.08865v4.

64. Prospects for Lepton Flavour Violation Measurements in  $\tau \rightarrow 3\mu$  Decays with the ATLAS Detector at the HL-LHC. Technical Report ATL-PHYS-PUB-2018-032, CERN, Geneva. 2018. Available online: <https://atlas.web.cern.ch/Atlas/GROUPS/PHYSICS/PUBNOTES/ATL-PHYS-PUB-2018-032> (accessed on 20 December 2023).
65. Crivellin, A.; Hofer, L.; Matias, J.; Nierste, U.; Pokorski, S.; Rosiek, J. Lepton-flavour violating  $B$  decays in generic  $Z'$  models. *Phys. Rev. D* **2015**, *92*, 054013. [[CrossRef](#)]
66. Crivellin, A.; Müller, D.; Signer, A.; Ulrich, Y. Correlating lepton flavor universality violation in  $B$  decays with  $\mu \rightarrow e\gamma$  using leptoquarks. *Phys. Rev. D* **2018**, *97*, 015019. [[CrossRef](#)]
67. de Medeiros Varzielas, I.; Hiller, G. Clues for flavor from rare lepton and quark decays. *JHEP* **2015**, *6*, 072. [[CrossRef](#)]
68. Hiller, G.; Loose, D.; Schönwald, K. Leptoquark Flavor Patterns & B Decay Anomalies. *JHEP* **2016**, *12*, 027. [[CrossRef](#)]
69. Hiller, G.; Loose, D.; Nišandžić, I. Flavorful leptoquarks at hadron colliders. *Phys. Rev. D* **2018**, *97*, 075004. [[CrossRef](#)]
70. Aaij, R.; Adeva, B.; Adinolfi, M.; Ajaltouni, Z.; Akar, S.; Albrecht, J.; Alessio, F.; Alexander, M.; Alfonso Albero, A.; Ali, S.; et al. Search for the lepton-flavour violating decays  $B_{(s)}^0 \rightarrow e^\pm \mu^\mp$ . *JHEP* **2018**, *3*, 078. [[CrossRef](#)]
71. Aaij, R.; Abdeltmotteleb, A.S.W.; Abellán Beteta, C.; Abudinén, F.; Ackernley, T.; Adeva, B.; Adinolfi, M.; Afsharnia, H.; Agapopoulou, C.; Aidala, C.A.; et al. Search for the lepton-flavour violating decays  $B^0 \rightarrow K^{*0} \mu^\pm e^\mp$  and  $B_s^0 \rightarrow \phi \mu^\pm e^\mp$ . *JHEP* **2023**, *6*, 073. [[CrossRef](#)]
72. Aaij, R.; Abellán Beteta, C.; Ackernley, T.; Adeva, B.; Adinolfi, M.; Aidala, C.A.; Ajaltouni, Z.; Akar, S.; Albicocco, P.; Albrecht, J.; et al. Search for Lepton-Flavor Violating Decays  $B^+ \rightarrow K^+ \mu^\pm e^\mp$ . *Phys. Rev. Lett.* **2019**, *123*, 241802. [[CrossRef](#)] [[PubMed](#)]
73. Aubert, B.; Barate, R.; Bona, M.; Boutigny, D.; Couderc, F.; Karyotakis, Y.; Lees, J.P.; Poireau, V.; Tisserand, V.; Zghiche, A.; et al. Measurements of branching fractions, rate asymmetries, and angular distributions in the rare decays  $B \rightarrow K \ell^+ \ell^-$  and  $B \rightarrow K^* \ell^+ \ell^-$ . *Phys. Rev. D* **2006**, *73*, 092001. [[CrossRef](#)]
74. Choudhury, S.; Sandilya, S.; Trabelsi, K.; Giri, A.; Aihara, H.; Al Said, S.; Asner, D.M.; Atmacan, H.; Aulchenko, V.; Aushev, T.; et al. Test of lepton flavor universality and search for lepton flavor violation in  $B \rightarrow K \ell \ell$  decays. *JHEP* **2021**, *3*, 105. [[CrossRef](#)]
75. Aubert, B.; Bona, M.; Boutigny, D.; Karyotakis, Y.; Lees, J.P.; Poireau, V.; Prudent, X.; Tisserand, V.; Zghiche, A.; Garra Tico, J.; et al. Search for the rare decay  $B \rightarrow \pi \ell^+ \ell^-$ . *Phys. Rev. Lett.* **2007**, *99*, 051801. [[CrossRef](#)]
76. Aaij, R.; Abellán Beteta, C.; Adeva, B.; Adinolfi, M.; Aidala, C.A.; Ajaltouni, Z.; Akar, S.; Albicocco, P.; Albrecht, J.; Alessio, F.; et al. Search for the lepton-flavour-violating decays  $B_s^0 \rightarrow \tau^\pm \mu^\mp$  and  $B^0 \rightarrow \tau^\pm \mu^\mp$ . *Phys. Rev. Lett.* **2019**, *123*, 211801. [[CrossRef](#)]
77. Aubert, B.; Bona, M.; Karyotakis, Y.; Lees, J.P.; Poireau, V.; Prudent, X.; Tisserand, V.; Zghiche, A.; Garra Tico, J.; Grauges, E.; et al. Searches for the decays  $B^0 \rightarrow \ell^\pm \tau^\mp$  and  $B^+ \rightarrow \ell^+ \nu$  ( $\ell = e, \mu$ ) using hadronic tag reconstruction. *Phys. Rev. D* **2008**, *77*, 091104. [[CrossRef](#)]
78. Atmacan, H.; Schwartz, A.J.; Kinoshita, K.; Adachi, I.; Adamczyk, K.; Aihara, H.; Al Said, S.; Asner, D.M.; Aulchenko, V.; Aushev, T.; et al. Search for  $B^0 \rightarrow \tau^\pm \ell^\mp$  ( $\ell = e, \mu$ ) with a hadronic tagging method at Belle. *Phys. Rev. D* **2021**, *104*, L091105. [[CrossRef](#)]
79. Aaij, R.; Abdeltmotteleb, A.S.W.; Abellán Beteta, C.; Abudinén, F.; Ackernley, T.; Adeva, B.; Adinolfi, M.; Afsharnia, H.; Agapopoulou, C.; Aidala, C.A.; et al. Search for the lepton-flavour violating decays  $B^0 \rightarrow K^{*0} \tau^\pm \mu^\mp$ . *JHEP* **2023**, *6*, 143. [[CrossRef](#)]
80. Aaij, R.; Abellán Beteta, C.; Ackernley, T.; Adeva, B.; Adinolfi, M.; Afsharnia, H.; Aidala, C.A.; Aiola, S.; Ajaltouni, Z.; Akar, S.; et al. Search for the lepton flavour violating decay  $B^+ \rightarrow K^+ \mu^- \tau^+$  using  $B_{s2}^{*0}$  decays. *JHEP* **2020**, *6*, 129. [[CrossRef](#)]
81. Lees, J.P.; Poireau, V.; Tisserand, V.; Garra Tico, J.; Grauges, E.; Milanes, D.A.; Palano, A.; Pappagallo, M.; Eigen, G.; Stugu, B.; et al. A search for the decay modes  $B^\pm \rightarrow h^\pm \tau \ell$ . *Phys. Rev. D* **2012**, *86*, 012004. [[CrossRef](#)]
82. Aaij, R.; Abellán Beteta, C.; Adeva, B.; Adinolfi, M.; Affolder, A.; Ajaltouni, Z.; Akar, S.; Albrecht, J.; Alessio, F.; Alexander, M.; et al. Search for the lepton-flavour violating decay  $D^0 \rightarrow e^\pm \mu^\mp$ . *Phys. Lett. B* **2016**, *754*, 167–175. [[CrossRef](#)]
83. Aaij, R.; Abellán Beteta, C.; Ackernley, T.; Adeva, B.; Adinolfi, M.; Afsharnia, H.; Aidala, C.A.; Aiola, S.; Ajaltouni, Z.; Akar, S.; et al. Searches for 25 rare and forbidden decays of  $D^+$  and  $D_s^+$  mesons. *JHEP* **2021**, *6*, 044. [[CrossRef](#)]
84. Lees, J.P.; Poireau, V.; Tisserand, V.; Grauges, E.; Palano, A.; Eigen, G.; Brown, D.N.; Kolomensky, Y.G.; Fritsch, M.; Koch, H.; et al. Search for lepton-flavor-violating decays  $D^0 \rightarrow X^0 e^\pm \mu^\mp$ . *Phys. Rev. D* **2020**, *101*, 112003. [[CrossRef](#)]
85. Lees, J.P.; Poireau, V.; Tisserand, V.; Grauges, E.; Palano, A.; Eigen, G.; Brown, D.N.; Kolomensky, Y.G.; Fritsch, M.; Koch, H.; et al. Search for Rare or Forbidden Decays of the  $D^0$  Meson. *Phys. Rev. Lett.* **2020**, *124*, 071802. [[CrossRef](#)] [[PubMed](#)]
86. Abouzaid, E.; Arenton, M.; Barker, A.R.; Bellantoni, L.; Bellavance, A.; Blucher, E.; Bock, G.J.; Cheu, E.; Coleman, R.; Corcoran, M.D.; et al. Search for lepton flavor violating decays of the neutral kaon. *Phys. Rev. Lett.* **2008**, *100*, 131803. [[CrossRef](#)] [[PubMed](#)]
87. Cortina Gil, E.; Kleimenova, A.; Minucci, E.; Padolski, S.; Petrov, P.; Shaikhiev, A.; Volpe, R.; Numao, T.; Petrov, Y.; Velghe, B.; et al. A search for the  $K^+ \rightarrow \mu^- \nu e^+ e^+$  decay. *Phys. Lett. B* **2023**, *838*, 137679. [[CrossRef](#)]
88. Cortina Gil, E.; Jerhot, J.; Lurkin, N.; Numao, T.; Velghe, B.; Wong, V.W.S.; Bryman, D.; Bician, L.; Hives, Z.; Husek, T.; et al. HIKE, High Intensity Kaon Experiments at the CERN SPS: Letter of Intent. *arXiv* **2022**, arXiv:2211.16586.
89. Aad, G.; Abbott, B.; Abdallah, J.; Abdel Khalek, S.; Abidinov, O.; Aben, R.; Abi, B.; Abolins, M.; AbouZeid, O.S.; Abramowicz, H.; et al. Search for the lepton flavor violating decay  $Z \rightarrow e\mu$  in pp collisions at  $\sqrt{s}$  TeV with the ATLAS detector. *Phys. Rev. D* **2014**, *90*, 072010. [[CrossRef](#)]
90. Aad, G.; Abbott, B.; Abbott, D.C.; Abed Abud, A.; Abeling, K.; Abhayasinghe, D.K.; Abidi, S.H.; Abou Zeid, O.S.; Abraham, N.L.; Abramowicz, H.; et al. Search for charged-lepton-flavour violation in Z-boson decays with the ATLAS detector. *Nat. Phys.* **2021**, *17*, 819–825. [[CrossRef](#)]

91. Aad, G.; Abbott, B.; Abbott, D.C.; Abed Abud, A.; Abeling, K.; Abhayasinghe, D.K.; Abidi, S.H.; Abramowicz, H.; Abreu, H.; Abulaiti, Y.; et al. Search for lepton-flavor-violation in  $Z$ -boson decays with  $\tau$ -leptons with the ATLAS detector. *Phys. Rev. Lett.* **2022**, *127*, 271801. [[CrossRef](#)] [[PubMed](#)]
92. Aad, G.; Abbott, B.; Abbott, D.C.; Abed Abud, A.; Abeling, K.; Abhayasinghe, D.K.; Abidi, S.H.; Abou Zeid, O.S.; Abraham, N.L.; Abramowicz, H.; et al. Search for the Higgs boson decays  $H \rightarrow ee$  and  $H \rightarrow e\mu$  in  $pp$  collisions at  $\sqrt{s} = 13$  TeV with the ATLAS detector. *Phys. Lett. B* **2020**, *801*, 135148. [[CrossRef](#)]
93. Sirunyan, A.M.; Tumasyan, A.; Adam, W.; Andrejkovic, J.W.; Bergauer, T.; Chatterjee, S.; Dragicevic, M.; Escalante Del Valle, A.; Frühwirth, R.; Jeitler, M.; et al. Search for lepton-flavor violating decays of the Higgs boson in the  $\mu\tau$  and  $e\tau$  final states in proton-proton collisions at  $\sqrt{s} = 13$  TeV. *Phys. Rev. D* **2021**, *104*, 032013. [[CrossRef](#)]
94. Aad, G.; Abbott, B.; Abbott, D.C.; Abeling, K.; Abidi, S.H.; Aboulhorma, A.; Abramowicz, H.; Abreu, H.; Abulaiti, Y.; Abusleme Hoffman, A.C.; et al. Searches for lepton-flavour-violating decays of the Higgs boson into  $e\tau$  and  $\mu\tau$  in  $\sqrt{s} = 13$  TeV  $pp$  collisions with the ATLAS detector. *JHEP* **2023**, *7*, 166. [[CrossRef](#)]

**Disclaimer/Publisher's Note:** The statements, opinions and data contained in all publications are solely those of the individual author(s) and contributor(s) and not of MDPI and/or the editor(s). MDPI and/or the editor(s) disclaim responsibility for any injury to people or property resulting from any ideas, methods, instructions or products referred to in the content.